1 Title: Basic and translational science of cyst wall proteins of the eye pathogen *Acanthamoeba* (87 characters +

2 spaces)

3 Short title: *Acanthamoeba* cyst wall proteins (32 characters + spaces)

4 Bharath Kanakapura Sundararaj[1], Manish Goyal[1], and John Samuelson[1]*

5 [1] Department of Molecular and Cell Biology, Boston University Goldman School of Dental Medicine, Boston,

6 Massachusetts, United States of America

7 *jsamuels@bu.edu

Abstract

The cyst wall of *Acanthamoeba castellanii* (Ac) contains cellulose and has outer ectocyst and inner endocyst layers connected by conical ostioles. Previously, we used mass spectrometry of purified Ac walls to identify families of abundant lectins (Jonah, Luke, and Leo). With the goal of identifying and characterizing novel target proteins for the diagnosis of cysts in patients with *Acanthamoeba* keratitis (AK), we localized three additional GFP-tagged proteins (a multicopper oxidase (AKA laccase) and additional Jonah and Leo lectins) to the ectocyst layer of the Ac wall. Although all walls proteins are expressed only during encystation, the precise timing of expression plays a decisive factor in their subcellular localization. Promoter swaps experiments showed early expression causes proteins to localize to the ectocyst layer, while later expression causes proteins to localize to the endocyst layer and ostioles. Ac wall proteins originate from bacteria by horizontal gene transfer (β-helical folds of Jonah and three cupredoxin-like domains of the laccase), share a common ancestry with wall proteins of slime molds (β-jelly-roll folds of Luke), or are unique to *Acanthamoebae* (four disulfide knots of Leo). β-jelly-roll folds of Luke and disulfide knots of Leo both share a linear array of aromatic amino acids, which are necessary for binding cellulose and proper localization of these proteins in the cyst wall, a feature consistent with convergent evolution. Purified rabbit antibodies to recombinant proteins bound to the ectocyst layer (Jonah and laccase) and/or to the ostioles (Luke and Leo) of cysts of 10 of 11 *Acanthamoeba* isolates tested, including five T4 genotypes that cause most cases of AK. In summary, we combined basic science experiments to understand better the localization, origin, and structure of Ac cyst wall proteins with translational studies to test target proteins for diagnosis of cysts in eye infections.

Author summary

Acanthamoebae are free-living amoeba in the soil and water that cause *Acanthamoeba* keratitis in under-resourced countries, where water for washing hands may be scarce. *Acanthamoeba* is an emerging pathogen in the United States, because of its association with contact lens use. While cysts are the primary target for diagnosing *Acanthamoeba* keratitis by microscopy of corneal scrapings, there are presently no diagnostic antibodies to characterize cyst wall proteins. Here we show that two Jonah lectins, a Leo lectin with a large spacer, and a laccase are present in the outer layer of the *Acanthamoeba* cyst wall, while Luke lectin and Leo without a spacer are present in the inner layer and the conical ostioles that connect the layers. We used structural predictions to identify the aromatic amino acids of Luke and Leo necessary for binding cellulose in the wall and to identify domains of Jonah and laccase useful for making recombinant proteins to immunize rabbits. Rabbit antibodies to Jonah, Luke, Leo, and laccase efficiently detected cysts of ten of 11 *Acanthamoeba* isolates, including five T4 genotypes that cause most keratitis cases. We conclude that four abundant wall proteins are each good targets for diagnostic anti-cyst antibodies.

41 **Introduction**

42 *Acanthamoeba* keratitis (AK), which leads to scarring and blindness, if not successfully treated, is
43 caused by free-living amoebae, named for acanthopods (spikes) on the surface of trophozoites [1-3]. In
44 immunocompromised patients, *Acanthamoebae* may cause encephalitis, which is frequently fatal [4]. AK is
45 associated with corneal trauma in the Middle East, South Asia, and Africa, where water for handwashing is
46 often scarce [5-9]. AK is associated with contact lens use in the US, Europe, and Australia and so
47 *Acanthamoeba* is on the NIAID list of Emerging Infectious Diseases/Pathogens [3, 10-12]. Regardless of the
48 place or the cause of infection, 18S RNA sequences show that the T4 genotype most often causes AK, while
49 other genotypes less frequently or never cause AK [13-16]. The whole genome of the Neff strain of
50 *Acanthamoeba castellanii* (Ac), a T4 genotype that is broadly studied, was sequenced, and proteins were
51 predicted and deposited in AmoebaDB [17, 18]. Recently, the Neff genome has been re-sequenced with long
52 reads to produce 33 chromosome-size assemblies, while protein prediction has been improved by
53 transcriptomes of trophozoites and organisms encysting for eight hours [19, 20].

54 Cyst walls, which form when trophozoites are starved of nutrients, protect free-living *Acanthamoebae*
55 from osmotic shock in freshwater or drying in the air [21, 22]. The cyst wall also makes *Acanthamoebae*
56 resistant to disinfectants used to clean surfaces, alcohol-based hand sanitizers, sterilizing agents in contact
57 lens solutions, and/or antibiotics applied to the eye [23-27]. While trophozoites cause damage to corneal
58 epithelial cells, AK is most often diagnosed by microscopic identification of cysts in corneal scrapings [1, 2, 28].
59 *Acanthamoeba* cysts are detected using calcofluor white (CFW) or wheat germ agglutinin (WGA), which bind
60 to cellulose and chitin, respectively, in their walls [29, 30]. Because CFW and WGA also react with walls of
61 plants, fungi, and other protists, they are suboptimal reagents that may lead to incorrect diagnosis of AK [31-
62 33]. The translational goal of the present study, therefore, is to identify abundant cyst wall proteins, which
63 might be targets for diagnostic antibodies. Antibodies to the *Acanthamoeba* wall might also be useful to detect
64 cysts in concentrated water samples, monitor contamination in contact lens solutions, test reagents for
65 cleaning reusable contact lenses, and/or test drugs that inhibit encystation.

66 Nearly 50 years ago, cellulose (β-1,4-linked glucose) was identified in *Acanthamoeba* cyst walls, which
67 has an outer ectocyst layer and an inner endocyst layer connected by conical ostioles [34, 35]. Because

68 *Acanthamoeba* has a chitin synthase and WGA binds to cyst walls, it is also likely that chitin (β-1,4-linked
69 GlcNAc) is also present [36]. No cyst wall proteins were known until we purified cyst walls from the Neff strain
70 of *Acanthamoeba castellanii* (Ac), which is a T4 genotype, and identified three families of cellulose-binding
71 lectins that we named Jonah, Luke, and Leo [29]. When a representative protein from each family was tagged
72 with green fluorescent protein (GFP) and expressed under its own promoter in transfected Ac, Jonah localized
73 to the ectocyst layer that is made early, while Luke and Leo localized to the endocyst layer and ostioles that
74 are made later [37, 38]. Anti-GFP antibodies showed Jonah-GFP is more accessible than Luke-GFP and Leo-
75 GFP, suggesting Jonah and other ectocyst proteins might be better targets for anti-cyst antibodies to diagnosis
76 AK by fluorescence microscopy of eye scrapings [29].

77 Here we performed basic science experiments to understand better the localization, origin, and
78 structure of Jonah, Luke, and Leo lectins, as well as an abundant laccase, as well as translational science
79 experiments to test their value as targets for antibodies to diagnose cysts in patients with AK. First, we
80 identified three additional Ac proteins in the ectocyst layer and used RT-PCR and promoter swaps to begin to
81 understand why proteins are located there versus the endocyst layer and ostioles. Second, we used AlphaFold
82 and Foldseek to better understand the structure and origin of wall proteins [39-41], and we made alanine
83 mutations to show linear arrays aromatic amino acids of Luke and Leo bind cellulose [42-47]. Third, we tested
84 rabbit antibodies (rAbs) to recombinant Ac cyst wall proteins against cysts of 10 other *Acanthamoeba* strains
85 and species, including five T4 genotypes that cause most cases of AK [13-16].

86 **Results**

87 **Localization of Jonah-3, Leo-S, and laccase-1 to the ectocyst layer of mature walls of Ac**

88 The goal here was to identify additional abundant Ac cyst wall proteins that localize to the ectocyst layer, which
89 is likely more accessible to diagnostic antibodies than the endocyst layer. Jonah family lectins are highly
90 abundant in cyst walls and have an N-terminal signal peptide followed by one or three choice-of-anchor A (CAA)
91 domains, which form β-helical folds (BHFs) (Fig 1A). Jonah-1 (ACA1_164810), which has a long, unstructured
92 Thr-rich domain in addition to a single BHF, is expressed early during encystation and localizes to the ectocyst
93 layer when tagged with GFP and expressed under its own promoter in transformed Ac of the Neff strain (ATCC
94 30010) (Fig 1A, 1B, and 1E) (Supporting Information S1 and S2) [29, 37-41]. The ectocyst layer is labeled with

95 WGA, which binds to chitin, while the endocyst layer and ostioles are labeled with CFW, which binds to cellulose
96 and/or chitin. Here we tested the localization of Jonah-3 (ACA1_157320), which contains three BHFs and was
97 very abundant in purified cyst walls [17, 18, 29]. While other cyst wall proteins contain a signal peptide but no
98 TMHs, Jonah-3-AmoebaDB contains 12 transmembrane helices (TMHs) (Fig 1A) [48, 49]. GFP-tagged Jonah-
99 3-AmoebaDB, which was expressed under its own promoter, localizes to punctate rings around each ostiole (Fig
100 1B and 1C). To test whether this ring-like localization of Jonah-3-AmoebaDB might be an artifact of incorrect
101 protein prediction, we used an unfinished transcriptome of encysting Ac to make Jonah-3(c) (corrected), which
102 contains three BHFs separated by unstructured, Ser-rich spacers (Fig 1A and 1F and Supporting Information
103 S1). An alignment of Jonah-3(c) and Jonah-3-AmoebaDB shows 12 TMHs in the latter derive from a series of
104 frameshifts rather than deletions or insertions. Further, Jonah-3(c)-GFP localizes to the ectocyst layer with an
105 identical appearance to that of Jonah-1-GFP (Fig 1D).

106 Luke-2 (ACA1_377670) and Luke-3 (ACA1_245650), which have two or three β-jelly-roll folds (BJRFs),
107 respectively, that are separated by unstructured, Ser-rich spacer(s), are expressed later during encystation and
108 localize to the endocyst layer and ostioles when tagged with GFP and expressed under their own promoters (Fig
109 2A, 2B, 2D, and 2E). Leo-A (ACA1_074730), which contains two adjacent sets of four disulfide knots (4DKs), is
110 also expressed later in encystation and localizes to the endocyst layer and ostioles when tagged with GFP (Fig
111 3A, 3B, and 3G). Here we tested the localization of Leo-S lectin (ACA1_188350), which contains two sets of
112 4DKs separated by a long, unstructured, Thr-rich spacer (Figs 3A and 3I). We used for a second time the
113 unfinished Ac transcriptome to make Leo-S(c) that corrects an eight amino acid deletion in the N-terminal 4DK,
114 which was identified by an alignment with other Leo-S lectins (Supporting Information file S1). Unlike Leo-A-
115 GFP, which localizes to the endocyst layer and forms a flat ring around the ostioles, Leo-S(c)-GFP localizes to
116 the ectocyst layer of mature cyst walls in a pattern like those of Jonah-1 and Jonah-3(c) (Fig 3F). Time course
117 studies of Leo-S(c)-GFP during the encystation showed that after 12 hours encystation, Leo-S(c)-GFP is present
118 in a dense set of secretory vesicles (SV in Fig 3D) that fill the cytosol of cells, which are rounded but lack a wall
119 (as shown by a failure to label with WGA or CFW). However, after 24 hours encystation, Leo-S(c)-GFP forms a
120 patchy distribution on a single-layered wall, which is labeled with both WGA and CFW (Fig 3E). After 48 hours,

121 Leo-S(c)-GFP has a homogeneous distribution in the ectocyst layer (data not shown), which is the same as Leo-
122 S(c)-GFP in mature cysts at 72 hours (Fig 3F).

123 The last protein tested was laccase-1 (ACA1_068450), which is a multicopper oxidase with three
124 cupredoxin-like domains (CuRO-1, CuRO-2 and CuRO-3) that is abundant in purified cyst walls of Ac (Figs. 4A
125 and 4E) [29, 50, 51]. Laccase-2(c) (ACA1_006180), the sequence of which we corrected using the unfinished
126 transcriptome, is much less abundant and so was not localized. GFP-tagged laccase-1 under its own promoter
127 localizes to the ectocyst layer of mature Ac walls with an appearance like those of GFP-tagged Jonah-1, Jonah-
128 3(c), and Leo-S(c) (Fig 4D). Like Leo-S(c)-GFP, laccase-1-GFP fills secretory vesicles of Ac encysting for 18
129 hours, when there is no wall labeled with WGA or CFW (Fig 4B). N.B. that the precise timing of secretory vesicles
130 and wall formation may vary by up to 6 hours, depending on the exact condition of trophozoites prior to placement
131 in encystation medium. Unlike Leo-S(c)-GFP, after 24 hours encystation laccase-1-GFP is homogeneously
132 distributed in the single layered wall of Ac, which becomes the ectocyst layer of mature cysts at 72 hours (Fig
133 4C and 4D).

134 In summary, we localized three new proteins to the ectocyst layer of the Ac cyst wall, one of which was
135 correctly predicted by AmoebaDB (laccase-1) and two of which needed to be corrected using an unfinished
136 transcriptome (Jonah-3(c) and Leo-S(c)). We also showed that Leo-S(c) and the laccase-1 are each made early
137 during encystation in a dense set of secretory vesicles, which are released onto the single-layered wall in a
138 fashion like that of Jonah-1 [29].

139 **RT-PCR and promoter swaps show timing of expression does not just correlate with but causes protein**
140 **localization in the ectocyst layer (earlier) or the endocyst layer and ostioles (later)**

141 The first goal here was to test the hypothesis that early expression does not just correlate with but causes Ac
142 cyst wall proteins to localize to the ectocyst layer, while later expression causes cyst wall proteins to localize to
143 the endocyst layer and ostioles [29]. The second goal was to determine whether proteins expressed under the
144 same promoter have the similar or different localizations in the Ac cyst wall, which would suggest similar or
145 different binding specificity, respectively, for cellulose and/or chitin, the two glycopolymers that form fibers in the
146 wall [35, 36]. For this, we performed qRT-PCR analysis to first determine the expression profile (timing of
147 expression) of individual lectins during encystation. RT-PCR with mRNA isolated from trophozoites and Neff

148 strain encysting for 96 hours, confirmed that Jonah-1 and laccase-1 are transcribed earlier during encystation,
149 while Luke-2 and Leo-A are transcribed later (Fig 5A). Note here that qRT-PCR products were normalized by
150 calreticulin, which is part of the *N*-glycan-dependent quality control of protein folding in the ER and is highly
151 expressed in trophozoites and encysting Ac [52]. The qRT-PCR results agree with those of the unfinished
152 transcriptome, which also suggests the low level of Leo-A is likely caused by a suboptimal choice of primers for
153 RT-PCR. Next, we performed the promoter swap experiments, in which we used GFP-tagged proteins that were
154 either made earlier and localized to the ectocyst layer (Jonah-1 and laccase-1), and/or made later and localize
155 to the endocyst layer and ostioles (Luke-2 and Leo-A) (Fig 1B, 2B, 3D to 3F, and 4B to 4D) [29].

156 In the first promoter swap experiment, we expressed Jonah-1-GFP (earlier) and Luke-2-GFP (later) each
157 under its own promoter or under the other promoter and then determined their localizations in mature Ac cyst
158 walls [29, 37, 38]. Jonah-1-GFP expressed under the later Luke-2 promoter moves from the ectocyst layer to the
159 ostioles, which are densely coated and increase in number from ~9 to as many as 16, while the endocyst layer
160 is weakly labeled (Fig 5B and 5C). The localization of Jonah-1-GFP under Luke-2 promoter is distinct from those
161 of GFP-tagged Luke-2 and Leo-A under their own promoters, which show much greater localization to the
162 endocyst layer, suggesting Jonah-1 binds to different glycopolymers (Fig 1B and 2B). Conversely, Luke-2-GFP
163 expressed under the earlier Jonah-1 promoter moves from the endocyst layer and ostioles to lightly decorate the
164 ectocyst layer and form flat, narrow rings around the ostioles (Fig 5D and 5E). These narrow rings, which match
165 those of Luke-2-GFP under its own promoter, suggest that the glycopolymer in the ostiole to which Luke-2 is
166 binding is available both earlier and later during encystation. The localization of Luke-2-GFP in the ectocyst layer
167 is distinct from those of GFP-tagged Jonah-1, Jonah-3(c), Leo-S(c), or laccase-1, which, under their own
168 promoters, coat the ectocyst layer and form dimples where ostioles are located (Fig 1B, 1D, 3F, and 4D). This
169 result suggests that glycopolymers bound by Luke-2 are likely not the same as those bound by proteins that
170 normally localize to the ectocyst layer.

171 In the second promoter swap experiment, we expressed laccase-1-GFP (earlier) and Leo-A-GFP (later)
172 each under its own promoter or the other promoter and determined their localizations in mature cyst walls.
173 Laccase-1-GFP expressed under the later Leo-A promoter moves from the ectocyst layer to the ostioles, which
174 are densely coated (Fig 5F and 5G). Leo-A-GFP expressed under the earlier laccase-1 promoter, moves from

175 the endocyst layer and ostioles to decorate lightly the ectocyst layer and form flat rings around the ostioles (Fig
176 5H and 5I). Of note, the locations of Jonah-1-GFP and laccase-1-GFP under both promoters resemble each
177 other but are distinct from locations of Luke-2-GFP and Leo-A-GFP under both promoters.

178 In summary, qRT-PCR support previous conclusions based upon GFP-tagged proteins that Jonah-1 and
179 laccase-1 in the ectocyst layer proteins are made earlier, while Luke-2 and Leo-A in the endocyst layer and
180 ostioles are made later [29]. Promoter swaps support our hypothesis that earlier expression does not just
181 correlate with but causes proteins to localize to the ectocyst layer and later expression causes proteins to localize
182 to the endocyst layer and ostioles. Promotor swaps also show that all four wall proteins can locate to ectocyst
183 and endocyst layers and ostioles, which has relevance to complicated patterns of binding of rAbs to Luke-2 and
184 Leo-A to cyst walls (see below). Finally, Jonah-1 and laccase-1 appear to bind to different glycopolymers than
185 Luke-2 and Leo-A.

186 **Structures of abundant wall proteins reveal the complex ancestry of Ac cyst wall proteins and identify**
187 **linear arrays of three aromatic amino acids in Luke-2 and Leo-A, which bind cellulose and direct proteins**
188 **to the Ac cyst wall**

189 Previously, we used sequence-based searches to show that Jonah lectins contain one or three choice of anchor-
190 A (CAA) domains like a spore coat protein of *Bacillus anthracis*, while Luke lectins contain two or three domains
191 similar to those of cellulose-binding proteins of *Dictyostelium discoideum* to carbohydrate-binding modules of
192 bacteria (CBM2) and plant (CBM49) endocellulases [29, 32, 42-45, 53-56]. Further, the Ac laccase-1 has three
193 cupredoxin-like domains like those of bacterial and fungal enzymes, while 8-Cys domains of Leo appear to be
194 unique to Ac [50, 51]. Here we used AlphaFold and Foldseek to 1) predict structures of abundant cyst wall
195 proteins and compare them to proteins with proven structures, 2) identify cellulose-binding sites for Luke and
196 Leo lectins, and 3) select domains in Jonah-1 and laccase-1 for immunizing rabbits to produce antibodies that
197 detect cysts by immunofluorescence microscopy [39-41].

198 Luke-2 and Luke-3 have two and three β-jelly-roll folds (BJRFs), respectively, each of which has a
199 disulfide bond linking its beginning to its end. The BJRFs of Luke lectins are separated by short (33 to 47-aa)
200 unstructured domains enriched in Ser (yellow) or Thr (blue) (Fig 2D and 2E). Slimes molds including
201 *Dictyostelium, Tieghemostelium, Heterostelium, Cavenderia*, and *Polysphondylium* also have cell wall proteins

202 with one to five similar BJRFs, consistent their shared ancestry with Luke lectins [32, 55]. Further, the BJRFs of
203 Luke-2 and a predicted *Dictyostelium* cellulose-binding protein (Q86KB6_DICDI) each contain a linear array of
204 three aromatic amino acids that are also present in CBM2 of an endocellulase of a cellulolytic soil bacterium
205 *Cellulomonas fimi,* the structure of which has been solved (PDB 1EXH) (pink arrows in Fig 2F and 2G) [57, 58].
206 Ala mutations of these three aromatic amino acids in CBM2 and in CBM49 of a plant endocellulase, which is
207 closely related, show they are the binding sites for cellulose [42, 47]. Here we muted to Ala two sets of three
208 aromatics (W35, W73, and W88 and W187, W228, and F244) of Luke-2, which was fused to maltose-binding
209 protein (MBP) and expressed in the periplasm of *E. coli* where, like the endoplasmic reticulum of eukaryotic cells,
210 disulfide bonds are formed [29, 59, 60]. We purified MBP-Luke-2 +/- Ala mutations on amylose resins and tested
211 their binding to Avicel (crystalline) cellulose. Western blots showed WT Luke-2 binds well to Avicel cellulose,
212 while MBP alone and Luke-2 plus Ala-mutations fail to bind to cellulose (Fig 2J). Further, Luke-2-GFP plus Ala
213 mutations, which was expressed under the same promoter as WT Luke-2-GFP, no longer localizes in the
214 endocyst layer and ostioles (Fig 2B and 2C). The binding of MBP-WT Luke-2 to Avicel cellulose argues for its
215 proper folding, so we used it to immunize rabbits.

216 Leo lectins have two sets of four disulfide knots (4DKs), which are adjacent (Leo-A) or separated by a
217 long, unstructured, Thr-rich domain (Leo-S(c)) (Fig 3G and 3I). Although there are numerous carbohydrate-
218 binding modules composed of sets of 4DKs (e.g., CBM18 of WGA, CBM19 of a *Saccharomyces cerevisiae* GH18
219 chitinase, and CBM55 of *Entamoeba histolytica* GH18 chitinase), we were unable with Foldseek to identify any
220 shared structures with the set of 4DKs of Leo [43, 46, 61-64]. Remarkably, 4DKs of Leo-A and Leo-S(c) contain
221 linear arrays of three aromatic residues, even though these 4DKs have no relationship to BJRFs of Luke or to
222 CBM2 and CBM49 of bacterial and plant endocellulases (Fig 3H). Ala mutations to two sets of three aromatics
223 (Y46, Y63, and Y77 and Y134, Y151, and Y165) caused an MBP-Leo-A fusion to no longer bind to Avicel
224 cellulose (Fig 2J). Similarly, the Ala mutant of Leo-A-GFP, which was expressed under the same promoter as
225 WT Leo-A-GFP, no longer localizes to the endocyst layer and ostioles (Fig 3B and 3C). As above, the binding of
226 MBP-WT Leo-A to Avicel cellulose argues for its proper folding, so we used it to immunize rabbits.

227 Jonah-1 has a single three-sided BHF, a pair of α-helices of unknown function, and a long, unstructured,
228 Thr-rich domain, while Jonah-3(c) has three BHFs and three long, unstructured, Ser-rich domains (Fig 1E and

229 1F). The BHF of Jonah-1 closely resembles the three-sided BHF of an antifreeze protein of an Antarctic sea ice
230 bacterium *Colwella sp*., the structure of which has been solved (PDB 3WP9) (Figs 1E to 1H) [65]. Although
231 Jonah-1 and laccase-1 (next paragraph) contained numerous aromatic amino acids on their surface, none was
232 in linear arrays, so we did not perform Ala mutations to test cellulose-binding. Finally, we chose the BHF of
233 Jonah-1 to make an MBP-fusion for immunizing rabbits, because we wanted to avoid unstructured, Thr-rich
234 regions, which might interfere with proper folding of the protein and/or contain *O*-linked glycans that would
235 obscure antigenic sites.

236 The laccase-1 of Ac has three cupredoxin-like domains (CuRO-1, CuRO-2 and CuRO-3) but lacks
237 unstructured, Ser- or Thr-rich domains, which distinguishes it from other ectocyst layer proteins (Jonah-1, Jonah-
238 3(c), and Leo-S(c)) (Fig 4E). Instead, laccase-1 has a positively charged loop between CuRO-2 and CuRO-3,
239 which is also present in spore coat proteins of bacteria. Ac laccase-1 shares a 44% identity with spore coat
240 protein A of *Caldicoprobacter faecalis*, which is present in sewage sludge. Ac laccase-1 shows slightly lower
241 positional identities with laccases of archaea (e.g., 40% with *Halalkalicoccus paucihalophilus*, fungi (e.g., 38%
242 identity with *Penicillium nalgiovense*), and plants (e.g., 36% with *Diphasiastrum complanatum* (36%). *Pelomyxa*
243 *schiedti* (36% identity) is the only Amoebazoa with a laccase, which is absent from humans and most metazoa
244 but are present in a few arthropods (e.g., 28% identity with *Rotaria sp.*). While the high positional identity with
245 bacterial laccases suggests the Ac laccase-1 may be active, we did not determine what substrates are oxidized,
246 and we did not knock it out to determine its function. The CuRO-1 of laccase-1, which we chose to make an
247 MBP-fusion for immunizing rabbits, closely resembles that of the spore coat protein A of *Bacillus subtilis*, the
248 structure of which has been solved (PDB 4YVN) (Fig. 4F) [66]. A possible concern here is the presence of a
249 10-aa sequence (NVYAGLAGFY) near the C-terminus, which is also present in laccases of some bacteria,
250 archaea, fungi, and plants and so might lead to cross-reacting antibodies.

251 In summary, BJRFs of Luke lectins share recent common ancestry with wall proteins of slime molds and
252 distant ancestry with CBM2 and CBM49 of bacterial and plant endocellulases, while 4DKs of Leo are unique.
253 BHFs of Jonah lectins and three CuRO domains of laccase closely resemble those of bacterial proteins and so
254 likely derive by horizontal gene transfer, which was not proven here. Although the structures of the BJRFs of
255 Luke-2 and the set of 4DKs of Leo-A show no resemblance, the linear arrays of three aromatic amino acids,

256 which are involved in binding cellulose and localizing proteins in the endocyst layer and ostioles, are the same,
257 consistent with convergent evolution. Finally, while the BHF of Jonah-1, BJRFs of Luke-2, and 4DKs of Leo-A
258 have no well-conserved sequences that might lead to cross-reacting antibodies with bacteria or fungi in eye
259 scrapings, CuRO-1 of laccase-1 has a well-conserved 10-aa sequence that may be problematic.

260 **Rabbit antibodies to Jonah-1, Luke-2, Leo-A, and laccase-1 all efficiently detect cysts of 10 of 11**
261 ***Acanthamoeba* isolates, including five T4 genotypes that cause most cases of AK.**

262 The goals here were to 1) use rAbs to recombinant wall proteins to visualize native proteins by western blots
263 and confocal microscopy and 2) test how well each antibody detected CFW-labeled cysts of 11 *Acanthamoeba*
264 species/strains.

265 Rabbits were immunized with MBP-fused to WT Luke-2, WT-Leo-A, BHF of Jonah-1, and CuRO-1 of the
266 laccase-1 in complete Freund's adjuvant and boosted three times with incomplete Freund's adjuvant at Cocalico
267 Biologics, Inc., and rabbit IgGs were purified using Protein-A Sepharose [59, 60]. Western blots and confocal
268 microscopy showed that pre-bleeds from rabbits do not react with trophozoites or cysts of Ac (Fig. 6A). While
269 rAbs to MBP-fusions with Jonah-1, Luke-2, Leo-A and laccase-1 do not bind to trophozoite proteins, each rAb
270 binds well to cyst wall proteins of Neff strain of Ac. Anti-Jonah-1 rAbs bind to a protein of the expected size of
271 ~55-kDa, as well as to two lower mol wt bands. The latter may result from proteolytic cleavage of Jonah-1 before
272 or during isolation of cyst proteins and/or by cross-reaction with smaller Jonah-1 proteins, which share multiple
273 conserved domains. Anti-Luke-2 rAbs bind to a thick ~50-kDa band, which is greater than the 27-kDa expected
274 size of Luke-2. We suspect that the increased size of Luke-2 is caused by extensive glycosylation of its five *N*-
275 glycan sites and ~20 *O*-glycan sites in the low complexity, Ser-rich spacer [67]. Anti-Leo-A rAbs bind to a thick
276 ~13-kDa band, which is slightly smaller than the expected size of 17-kDa, perhaps due to proteolytic cleavage.
277 Finally, anti-laccase-1 rAbs bind to a 75-kDa band, which is slightly bigger than the expected size of 64-kDa, as
278 well as to a less abundant 55-kDa band. Again, addition of *N*-glycans or *O*-glycans may explain the increase in
279 size, while proteolytic cleavage may explain the lower mol wt band.

280 We tested rAbs versus the model Neff strain of Ac, as well as *Acanthamoeba* species/strains from the
281 ATCC collected by Monica Crary, who studies their binding to contact lenses [24, 27]. Segments of 18S RNA
282 genes were amplified from trophozoites, cloned, and sequenced to confirm the genotype of 11 *Acanthamoeba*

283 species/strains prior to encystation and testing with rAbs [13-16]. Four T4 genotypes from the ATCC included *A.*
284 *castellanii* Neff stain (30010), MA strain (50370), and unnamed strain (50324) and *A. polyphaga* (30872), while
285 a fifth T4 (MEEI 0184) and another AK isolate (Esbc4) came from Noorjahan Panjwani, who discovered the
286 mannose-binding protein on the surface of trophozoites [68]. Other genotypes from ATCC included T7 (*A.*
287 *astronyxis* 30137), T11 (*A. hatchetti* PRA-115) and T18 (*A. byersi* PRA-411 and *Acanthamoeba sp. 13* 50655).

288 High-power confocal microscopy showed rAbs to the BHF of Jonah-1 bound in a somewhat patchy
289 distribution to the ectocyst layer (surface) of cysts of Neff strain and 10 other *Acanthamoeba* species and/or
290 strains (Fig 6A and 7A). This patchy distribution, which is in contrast to the homogeneous distribution of Jonah-1-
291 GFP (Fig 1B), may result from masking of the BHF of Jonah-1 by its large, unstructured Thr-rich domain, which
292 likely contains *O*-linked glycans, and/or masking by other ectocyst wall proteins (Fig 1E). In contrast, rAbs to
293 CuRO-1 of laccase-1 bound in a homogenous pattern to the Neff strain and to other *Acanthamoeba*
294 species/strains, which is similar to that of laccase-1-GFP, suggesting there is less masking of laccase-1 (Fig 4D,
295 6E, and 7D). While rAbs to Luke-2 and Leo-A densely labeled the ostioles and weakly labeled the endocyst layer
296 of many cysts (Figs. 6C and 6D), other cysts were labeled on the endocyst layer and/or ectocyst layer (Fig. 7B
297 and 7C). Of note, rAbs to Luke-2 and Leo-A often bound in similar patterns to a particular *Acanthamoeba* isolate,
298 which is reminiscent of similar appearances of Luke-2-GFP and Leo-A-GFP in the promoter swap experiments
299 (Fig 5). There are two explanations, which are not mutually exclusive, for the variable distribution in the cyst
300 walls of rAbs to Luke-2 and Leo-A. First, these proteins may be made at different times by different
301 *Acanthamoeba* species/strains, so that Luke-2 and Leo-A localize to different places. Second, these rAbs may
302 bind to relatively small amounts of Luke-2 and Leo-A in the ectocyst layer, which was not visualized by confocal
303 microscopy, because of the large amounts of GFP-tagged Luke-2 and Leo-A in the endocyst layer and ostioles
304 (Fig 2B and 3B).

305 To determine which wall proteins might be the best targets for diagnosis of cysts in AK, we counted in
306 randomly selected low power confocal fields the number of CFW-labeled cysts detected by rAbs to Jonah-1,
307 Luke-2, Leo-A, and laccase-1 (Fig 6F to 6I). In two separate experiments, >100 cysts were counted for each rAb
308 and each *Acanthamoeba* species/strain, and the averages +/- SEM were plotted in Fig 6J. We found that rAbs
309 to Luke-2, Leo-A, and laccase-1 each detected >95% of CFW-labeled cysts of 10 of 11 *Acanthamoeba* species

310 and strains tested. In contrast, anti-Jonah-1 rAbs showed >95% detection for 7 of 11 *Acanthamoeba* species but
311 detected somewhat fewer cysts of *A. byersi* (PRA-115) (T11) (91%), *Acanthamoeba* sp. 13 (ATCC 50655) (T18)
312 (89%), and *A. polyphaga* (ATCC 30872) (T4) (85%). Why this is the case is not clear, but the result, which
313 suggests that the BHF of Jonah-1 might not be quite as good a target as the BJRFs of Luke-2, the 4DKs of
314 Leo-A, or CuRO-1 of laccase-1, was reproduced in separate experiments. In addition, all four rAbs struggled to
315 detect *A. mauritaniensis* (T4) (ATCC 50676), suggesting that there is a problem with encysting these
316 trophozoites under the conditions used here. While counts were performed for two sets of cysts labeled with
317 Protein-A Sepharose-purified antibodies, we obtained similar results with rabbit sera diluted 1:300. Most
318 important, we confirmed that rAbs to all four proteins were also visible with a conventional Zeiss fluorescence
319 microscope, which is more similar to those present in clinical labs or in ophthalmologists' offices. While the
320 success with rAbs to Jonah-1 and laccase-1 was expected, because these proteins are on the ectocyst layer
321 (surface) of cysts, the success of rAbs to Luke-2 and Leo-A was unexpected because we previously had trouble
322 locating Luke-2-GFP or Leo-A-GFP using anti-GFP antibodies [29]. Finally, regardless of whether the rAbs are
323 binding to the ectocyst layer or endocyst layer, the presence of ~10 ostioles makes *Acanthamoeba* cysts look
324 distinct from fungal walls, which may at most have a few bud scars [29, 31, 34].

325 **Discussion**

326 **Incorrect protein prediction of Jonah-3 in AmoebaDB led to its art factual but interesting localization in**
327 **rings around ostioles**

328 While Ac proteins sequences available in AmoebaDB made it possible for us to perform mass spectrometry of
329 cyst walls and for others to discover dozens of proteins of interest, its predictions are based upon an incomplete
330 genome of Neff strain of Ac and algorithms that identify exons in genes with a high density of introns rather than
331 transcriptomic data [17, 18, 29]. We used an unfinished transcriptome to show TMHs between three BHFs,
332 which incorrectly localized GFP-tagged Jonah-3-AmoebaDB to a ring around ostioles, were caused by
333 frameshifts. Instead, Jonah-3(c) has low-complexity, Ser-rich spacers like those of Luke-2 and localizes to the
334 ectocyst layer in a pattern matching that of Jonah-1. The unfinished transcriptome also allowed us to correct an
335 eight amino acid long deletion in Leo-S-AmoebaDB that would have disabled its N-terminal 4DK, which is
336 necessary for binding cellulose and localizing the protein to the ectocyst layer. Because AmoebaDB predicts

337 14,000 proteins, the errors described here in Jonah-3, Leo-S, and laccase-2 are mere anecdotes but suggest a
338 need for a reannotated proteome based upon a well-constructed transcriptome. Finally, despite being an artifact,
339 rings around the ostioles formed by Jonah-3-AmoebaDB may be useful for studying ostiole formation during
340 encystation and ostiole breakdown during encystation. Similarly, the heavy labeling of ostioles by Jonah-1 and
341 laccase-1 under the later Luke-2 and Leo-A promoters, respectively, may also facilitate studies of ostiole
342 formation and degradation.

343 **Timing of expression and properties of abundant wall proteins determine their localization in the**
344 **ectocyst layer, endocyst layer, and/or ostioles**

345 Because whole cyst walls were purified by Percoll gradients and examined by mass spectrometry, we expressed
346 selected proteins with a GFP-tag under their own promoters to precisely localize them in the two layered-wall
347 connected by ostioles [29, 37, 38]. Here we increased the number of ectocyst layer proteins from one (Jonah-1)
348 to three (Jonah-3(c), Leo-S(c), and laccase-1. Laccase-1 and Leo-S(c) were also localized to a massive set of
349 secretory vesicles early in encystation, as was previously shown for Jonah-1. Rabbit antibodies confirmed the
350 presence of Jonah-1 and laccase-1 in the ectocyst layer of untransformed cysts of the model Neff strain of Ac,
351 as well as cysts of 10 other *Acanthamoeba* species/strains. Promoter swaps showed Jonah-1 and laccase-1
352 switch to the endocyst layer and ostioles when expressed under later promoters of Luke-2 and Leo-A,
353 respectively. Conversely, Luke-2 and Leo-A switch from the endocyst layer and ostioles to the ectocyst layer
354 when expressed under the early promoters of Jonah-1 and laccase-1, respectively. Because the localizations of
355 Jonah-1 and laccase-1 resemble each other under early and later promoters, it is likely that they are binding to
356 the same glycopolymer(s), which we did not determine here. Similar localizations of Luke-2 and Leo-A under
357 both promoters suggest these lectins are also binding to the same glycopolymer(s). This result is not surprising,
358 as Luke-2 and Leo-A contain similar arrays of aromatic amino acids that bind cellulose.

359 Our conclusion that early expression causes proteins to localize in the ectocyst layer, and later expression
360 causes proteins to localize in the endocyst layer and ostioles leaves many questions unanswered. As above, we
361 do not know how ostioles are formed, and we have not yet precisely localized cellulose and chitin in cyst walls.
362 Further, we have not identified sequences in regions 5' to the start ATG that bind transcription factors specific

363 for earlier or later encystation-specific expression, nor have we figured out why some encystation-specific
364 promoters are stronger than others and so produce greater quantities of transcripts for wall proteins.

365 **While its 4DKs are unique, Leo lectins share many properties with wall proteins of Ac and other**
366 **organisms, arguing for convergent evolution**

367 Although the four families of Ac wall proteins show no relationship to each other, three have been previously
368 identified and characterized in walls of protists, fungi, plants, and bacteria. Luke lectins have two or three BJRFs,
369 which share recent ancestry with wall proteins of *Dictyostelium* and distant ancestry with CBM2 and CBM49 of
370 bacterial and plant endocellulases [32, 42, 47, 55, 58]. Laccases, which are most similar to those of bacteria,
371 are widely distributed in walls of plants, fungi, and oomycetes [50, 51, 66]. Although their function in Ac, which
372 proliferate in temperate climates, is not clear, BHFs similar to those in Jonah lectins protect Artic bacteria from
373 freezing [56, 65]. While its 4DKs that bind cellulose are unique, Leo lectins share properties with wall proteins of
374 Ac and other organisms, suggesting the importance of convergent evolution [69]. Chitin-binding domains of
375 *Saccharomyces* chitinases (CBM19), *Entamoeba* chitinases (CBM55), and WGA (CBM18) also contain unique
376 4DKs, while chitin-binding domains of Jacob lectins contain unique 3DKs [43, 46, 62-64]. Even though 4DKs of
377 Leo and BJRFs of Luke have no structural similarity, each contains linear arrays of three aromatic amino acids,
378 which Ala mutations showed bind cellulose. Similar linear arrays of aromatics that bind cellulose are present in
379 endocellulases of bacteria (CBM2) and plants (CBM49), as well as in CBM63s of expansins (proteins that unfold
380 cellulose) of plants, bacteria, and Ac [42, 44, 47]. Reinvention by convergent evolution of these linear arrays of
381 aromatics strongly suggests they are the best means for binding cellulose, which forms flat ribbons with
382 alternating glucose residues facing opposite surfaces.

383 Like Leo-A with two adjacent 4DKs and Leo-S with 4DKs separated by a large Thr-rich spacer,
384 *Entamoeba* Jacob-1 has two adjacent 3DKs, while Jacob-2 has a third 3DK separated by a long, unstructured,
385 Ser-rich spacer [70]. Unstructured Ser- or Thr-rich domains, which are also present in Jonah and Luke lectins,
386 are likely modified by *O*-linked glycans, which protect glycoproteins from being degraded by bacterial proteases,
387 as shown for wall proteins of *Entamoeba* and *Cryptosporidium* [71, 72]. Due to constraints on resources and
388 time, we did not identify *O*-linked glycans on Ac cyst wall proteins, nor did we confirm the AlphaFold structures
389 by crystallizing any of the four wall proteins studied here. This seems less of an issue for the BHFs of Jonah-1

390 and -3, BJRFs of Luke-2 and Luke-3, and CuRO-1 domain of laccase-1, the structures of which match those of
391 crystallized proteins [58, 65, 66]. A goal of future studies will be to solve the crystal structure of the unique 4DK
392 of Leo +/- cellulose.

393 **Abundant wall proteins do not have to be in the ectocyst layer to be good targets for diagnostic**
394 **antibodies**

395 While it is rare for us (and other parasitologists) to pair basic and translational science experiments, it worked
396 well here for the following reasons. The BHF of Jonah-1, the BJRFs of Luke-2, the 4DKs of Leo-A, and CuRO-1
397 domain of laccase-1 each expressed well as MBP-fusions in the periplasm of bacteria, where disulfide bonds
398 are formed [59, 60]. In contrast to anti-peptide rAbs to Jonah-1 and Leo-A, which bound to Western blots but not
399 to fixed cysts [29], rAbs to MBP-fusions of all four Ac wall proteins bound well to Western blots and to cysts of
400 Neff strain of Ac, as well as to cysts of 9 of 10 other isolates of *Acanthamoeba*. While we expected that rAbs to
401 Jonah-1 and laccase-1, which are both in the accessible ectocyst layer, to efficiently detect CFW-labeled cysts,
402 anti-laccase-1 performed slightly better than anti-Jonah-1. Even though we doubted whether rAbs to Luke-2 and
403 Leo-A, which are in the relatively inaccessible endocyst layer and ostioles, would detect CFW-labeled cysts
404 efficiently, anti-Luke-2 and anti-Leo-A rAbs both performed very well. Although the labeling of the ectocyst layer
405 by rAbs to Luke-2 and Leo-A is not easy to explain, efficient detection is what matters for a diagnostic reagent.
406 Finally, the signal from the secondary goat antibody binding to rAbs to Jonah-1, Luke-2, Leo-A, and laccase-1 is
407 strong enough, so that cysts were easily detected with a conventional fluorescence microscope, not just by an
408 expensive confocal microscope used to get three-dimensional, high-resolution images of the ectocyst layer,
409 endocyst layer, and ostioles.

410 Because these rAbs cross-react with MBP that was not removed prior to vaccination, they are not ready
411 for testing on corneal scrapings that likely contain numerous bacteria. Although we are confident that Luke-2,
412 Leo-A, and Jonah-1 antigens are each unique to Ac, a 10-aa sequence in laccase-1 may lead to antibodies that
413 cross-react with walls of bacteria, fungi, or plants. Cysts examined here were made by starving cultured
414 *Acanthamoebae* and so might not be the same as those made in the corneal epithelium, soil, or water. Diagnostic
415 anti-cyst antibodies will complement monoclonal antibodies to the mannose-binding proteins on trophozoites
416 [68, 73], as well as antibodies to transporters and secreted proteins of trophozoites and cysts [74-76]. Anti-cyst

417 antibodies may also supplement Loop-mediated Isothermal Amplification (LAMP) assays for diagnosing AK [77,
418 78].

419 **METHODS**

420 **Ethics statement**

421 Culture and manipulation of *Acanthamoebae* under BSL-2 protocols were approved by the Boston University
422 Institutional Biosafety Committee. Production of custom rabbit antibodies was approved by the Institutional
423 Animal Care and Use Committee of Cocalico Biologics, Inc., Denver PA.

424 **Summary of new methods to study Ac wall proteins.**

425 Many methods are the same that we used in our mass spectrometric characterization of proteins in purified cyst
426 walls of Ac, which were described in detail [29]. New here is use of unfinished transcriptome to correct protein
427 prediction in AmoebaDB for Jonah-3(c) and Leo-S(c). Confocal microscopy replaced structured illumination
428 microscopy (SIM), because it is quicker and allowed us to examine many more parasites. Two pairs of promoter
429 swaps were used to show that localization in the two layers of the wall is not just correlated with timing of
430 expression but is caused by timing of expression. AlphaFold was used to predict structures for each cyst wall
431 protein and test with Ala mutations aromatic amino acids involved in binding cellulose. Foldseek was used to
432 suggest the origin of domains in cyst wall proteins that could not be identified using sequence-based searches.
433 Recombinant proteins, rather than peptides, were used to make rAbs to abundant wall proteins, which supported
434 localizations of four GFP-tagged constructs under their own promoters. Binding of the rAbs to cysts of numerous
435 *Acanthamoeba* genotypes, which were confirmed by PCR of 18S RNA genes, supported their use as targets for
436 diagnostic antibodies.

437 ***Acanthamoeba* species and strains, culture, and cyst preparation**

438 *A. castellanii* Neff strain (ATCC 30010) trophozoite parasites were obtained from the American Type Culture
439 collection (ATCC). Trophozoites of other strains of *Acanthamoeba*, originally derived from human corneal
440 infections and granulomatous encephalitis infections, were acquired from Dr. Monica Crary, Alcon Research,
441 LLC, Fort Worth, TX, United States or from Noorjahan Panjwani of Tufts University Medical School [24, 68]. All
442 experiments were performed using *A. castellanii* Neff strain until otherwise mentioned.

443 Ac trophozoites were grown and maintained in axenic culture at 30ºC in T-75 tissue culture flasks in 10
444 ml ATCC medium 712 (PYG plus additives) with antibiotics (Pen-Strep) (Sigma-Aldrich Corporation, St. Louis,
445 MO) as described previously [21, 29, 79]. Adherent log-phase trophozoites from stationary culture were detached
446 with the help of a cell scraper and pelleted down by centrifugation at 500x g for 5 min followed by two washes
447 with 1X phosphate buffered saline (PBS). Cysts were prepared from trophozoites by incubating them with
448 encystation medium (EM, 20 mM Tris-HCl [pH 8.8], 100 mM KCl, 8 mM $MgSO_4$, 0.4 mM $CaCl_2$, and 1 mM
449 $NaHCO_3$) [29, 79]. In brief, ~10^7 trophozoites obtained from a confluent flask were washed with 1x PBS and
450 subsequently incubated with EM in a T-75 tissue culture flask for 120 hours. The mature cysts were released
451 with the help of a cell scrapper, harvested, and washed with 1x PBS by centrifugation at 1,500x g for 10 min.
452 The harvested cysts were either used immediately or stored at 4ºC or -20ºC depending upon the need of the
453 experiment.

454 ***In silico* sequence analysis of candidate cyst wall lectins**

455 The full-length coding sequence of different cyst wall proteins of *A. castellanii* namely Jonah-1 (ACA1_16481),
456 Jonah-3 (ACA1_157320), Luke-2 (ACA1_377670), laccase-1 (ACA1_068450), Leo-A (ACA1_074730) and Leo-
457 S (ACA1_188350) were obtained from AmoebaDB, a functional genomic database useful for genetic studies of
458 the Neff strain and ten other *Acanthamoeba* strains (https://amoebadb.org/amoeba/app) [80]. The AmoebaDB
459 database was also used to predict introns and identify paralog proteins and upstream promoters (nucleotide
460 sequence) of different cyst wall proteins. The full-length amino acid sequences of candidate wall proteins were
461 further analyzed, reannotated, and corrected based on homologs proteins using BLAST server in other species
462 [53]. Other *in-silico* tools used to functionally characterize the cyst wall proteins include the CDD database
463 (conserved domain identification) [81], SignalP 4.1 [49] and DeepTMHMM [82] (signal peptides and
464 transmembrane helices), CAZy and InterPro databases (Carbohydrate-binding modules) [43, 46, 54] [48] and
465 big-PI (Glycosylphosphatidylinositol anchors) [83], respectively. Finally, we used an unfinished transcriptome of
466 trophozoites and encysting Ac, which will be described elsewhere when completed, to check and correct protein
467 predictions.

468 ***In silico* structural prediction of candidate cyst wall proteins**

469 The 3D structure models of different cyst wall lectins were predicted by AlphaFold2 using the Colab server
470 (https://colab.research.google.com/github/sokrypton/ColabFold/blob/main/AlphaFold2.ipynb) [39]. The
471 molecular visualization of active site residues, 3D structures, and structural superimposition was performed with
472 the help of PyMOL Molecular Graphics System, Version 2.0 Schrödinger, LLC [84]. Additionally, the predicted
473 3D structures were used to perform structural comparison and similarity search with large structure sets
474 (AlphaFold database, PDB database, etc.) using Foldseek server (https://search.foldseek.com/search) [40].

475 **Expression and localization of candidate cysts wall lectins during encystation in *A. castellanii***

476 RT-PCR studies were performed to check the expression of cyst wall lectins in encysting protists. In brief,
477 adherent log-phase trophozoites of Ac were washed twice with PBS and subsequently stimulated to encyst by
478 incubation at 30ºC with encystation media. The amoeba cells were collected at various time points including 0,
479 6, 12, 18, 24, 36, 48, 72, and 96 hours post incubation. The cells were pelleted down by centrifugation, washed
480 with PBS, and stored in Trizol reagent at -80ºC for further use. Once all the time points were collected, the Trizol
481 cell pellets were thawed on ice, and the cells were lysed by bead beating (BioSpec mini bead beater) operated
482 in a cold room at 4ºC with 1 min beating and cooling off for 5 mins for 3 cycles. Total RNA was extracted using
483 Directzol RNA minprep kit (Zymo Research), and the concentration was checked using Nanodrop 2000/2000c
484 (Thermo Fisher Scientific). cDNA was synthesized using AMV reverse transcriptase (New England Biolabs,
485 Ipswich, MA) as per the manufacturer instructions. The expression of abundant cyst wall proteins during
486 encystation was analyzed using Realtime-PCR (Biorad) using Power SYBR green PCR master mix (Applied
487 Biosystems). Calreticulin was used as housekeeping gene to normalize the expression profile of various
488 candidate cyst wall lectins. The primers used for real time PCR analysis are listed in Supporting Information S1.

489 To verify the expression and subcellular localization of cyst wall proteins during encystation, we
490 expressed individual cyst wall lectins from an episomal plasmid in Neff strain of Ac under their own promoter.
491 Primers for making constructs are listed in Supporting Information S1, while sequences of promoters and
492 proteins are listed in Supporting Information S2. For all constructs, the pGAPDH plasmid was used, which
493 harbors a neomycin resistance gene (for G418 drug selection) and a glyceraldehyde 3-phosphate
494 dehydrogenase (GAPDH) promoter for constitutive expression of a C-terminus GFP fusion chimera [37]. In our
495 *in silico* structural studies, we observed a comparable binding site topography for Luke-2 and Leo-A cellulose-

496 binding module (CBM), which consists of a linear array of aromatic amino acids, as previously observed
497 phenomenon for other CBMs. To confirm the involvement of these aromatics in Luke-2 and Leo-A CBMs these
498 aromatic amino acid residues were mutated to alanine. Tryptophan (W35, W73, W88, W187, W228 and
499 phenylalanine (F244) of Luke-2 were replaced with alanine, while tyrosine (Y46, Y63, Y66, Y134, Y151, and
500 Y165) of Leo-A were replaced with alanine. The construct used for Jonah-1, Leo-A (WT), and Luke-2 (WT) were
501 taken from a previously published study [29]. While the full-length coding sequences of Leo-A mutant, Luke-2
502 mutant, laccase-1, and Leo-S gene were codon optimized and custom synthesized from the Twist Biosciences
503 along with their respective promoter sequences. For the promoter swap experiment, the Luke-2 promoter was
504 replaced with Jonah-1, while the laccase-1 promoter was replaced with the Leo-A promoter and vice versa. The
505 5' upstream sequence (400-600 bp) (Supporting Information S2) for each gene was PCR amplified from Ac
506 genomic DNA (used as a promoter to drive their expression) to swap the respective gene promoter in the
507 pGAPDH plasmid. For construct preparation, we used a restriction-free cloning strategy using NEBuilder HiFi
508 DNA assembly master Mix from New England Biolabs, Ipswich, MA. The identities of final constructs were
509 sequence verified using Oxford nanopore sequencing technology from Plasmidsaurus. The primers used for
510 cloning of different promoters, and cyst wall lectin genes are listed in Supporting Information S1.

511 **Transfection**

512 Transfection in *A. castellanii* was performed routinely in the lab using Lipofectamine™ Transfection Reagent
513 (Thermo Fisher Scientific), as per the manufacturer's instruction. Briefly, for each transfection ~5 x 10^5 log-phase
514 trophozoites were seeded in a T-25 flask in ATCC medium 712 and incubated for 30 min at 30ºC. After the
515 incubation, the adherent trophozoites were washed, and the media was replaced with 500 µl of encystation
516 media (EM). Prior to transfection, the Lipofectamine™ 3000 reagent was diluted in EM (7.5 µL Lipofectamine™
517 3000 was diluted in 125 µL EM). The master mix of DNA was prepared by diluting 8 µg of plasmid DNA with EM
518 (to achieve a final volume of 117 µL) and subsequent addition of 8 µL P3000™ reagent. Diluted Lipofectamine™
519 3000 and DNA master mix both were added in a 1:1 (125 + 125 µl) ratio and incubated at room temperature for
520 an additional 15 min. Following incubation, the DNA-lipofectamine complex (250 µL) mixture was added directly
521 onto the adherent trophozoites in 1 mL EM (1250 µL). The trophozoites were further incubated for an additional
522 4 hours at 30ºC. After this, the EM and transfection mixture was removed by pipetting and 10 ml fresh media

523 was added into each well. After 24h of transfection, the used medium was replaced with fresh media containing
524 G418 (12.5 µg/mL). After 48h of transfection, cells were transferred from 6 well plates to T-75 flasks with ATCC
525 medium 712 plus G418 (25 µg/mL). The used medium was changed routinely with fresh media containing G418
526 (25 µg/mL) on every fourth day. After 2 to 4 weeks, the transfectants began growing robustly in the presence of
527 G418.

528 **Confocal microscopy**

529 To check the expression of the abundant cyst wall proteins during the encystation, the transgenic Ac trophozoites
530 (which express GFP-tagged chimera cyst wall proteins) were induced to encyst with EM. The encysting amoebas
531 were collected at various time points (0, 6, 12, 18, 24, 36, 48, 72, and 96 hours), centrifuged, washed (1x PBS),
532 and fixed by incubating them with 4% paraformaldehyde (PFA) for 15 min at room temperature. Following fixation
533 cells were pelleted down, washed, and resuspended in PBS. The fixed cells were stained with Wheat Germ
534 Agglutinin 1:10 (WGA, 1 mg/ml, ThermoFisher Scientific) conjugated to Alexa Flour 647 and Calcofluor White
535 1:20 (CFW, 1mg/ml, Sigma Aldrich) in PBS for 30 min at room temperature. The cells were washed 3 times with
536 1x PBS and mounted in VECTASHIELD® Antifade Mounting Medium (Vector Laboratories, Newark, CA).
537 Samples were illuminated using 380 nm (CFW), 488 nm (GFP chimera), and 647 nm (WGA) laser excitation. .
538 The fluorescence images were captured using CFI Plan Apochromat VC 60XC WI Plan APO 60x oil objective of
539 Nikon Ni2 AX inverted confocal microscope equipped with NIR imaging system. We deconvolved 0.1 µm optical
540 sections using NIS elements (Version: AR5.41.02) imaging software. All confocal images shown were 3D
541 reconstructions using dozens of z-stacks. Size bars were based upon 2D cross-sections.

542 **Overexpression and purification of candidate cyst wall proteins as MBP-fusion**

543 The MBP-fusion constructs of Jonah-1, laccase-1, Luke-2 (WT and mutant), and Leo-A (WT and mutant) were
544 prepared by cloning the codon-optimized (*E.coli* expression) synthetic gene fragments into pMAL-p2x vector
545 (New England Biolabs) for periplasmic expression in BL21-CodonPlus(DE3)-RIPL (Agilent Technologies,
546 Lexington, MA) [60]. The primers used for cloning synthetic gene fragments and the length of different domains
547 of cyst wall proteins (devoid of signal sequence) are listed in Supporting Information S1 and S2. The expression
548 of each MBP-fusion proteins was induced by the addition of 0.1 mM of IPTG for 16 h at 16°C. The bacterial cell
549 pellet was lysed, and supernatant was collected as per the manufacturer's specifications (New England Biolabs).

550 AKTA start was used to purify the MBP tagged protein using an MBPtrap HP column (Cytiva). The MBPtrap
551 column was equilibrated with equilibration or wash buffer (20 mM Tris-HCl (pH 8), 200 mM NaCl, 1 mM EDTA).
552 Later the supernatant mixture was passed through the column for the MBP-tagged protein to bind to the column
553 at 0.5 mL/min flow rate. The column washed with 20 column volumes of wash buffer, and the purified protein
554 was eluted with elution buffer (20 mM Tris-HCl (pH 8), 200 mM NaCl, 1 mM EDTA, 10 mM maltose). The identity
555 and purity of recombinant purified MBP-fusion proteins were confirmed by SDS-PAGE and Western
556 immunoblotting analyses. The wild-type recombinant Jonah-1, Luke-2, Leo-A, and laccase-1 MBP-fusions were
557 used to raise custom polyclonal antibodies (Cocalico Biologicals). Total IgG was purified from plasma samples
558 of pre-immune and post-immunized rabbits via Protein A affinity chromatography (Pierce™ Protein A Agarose,
559 Thermo Fisher Scientific, USA) as per manufacturer instructions. In brief, for Protein A Sepharose purification,
560 plasma was diluted 2-fold with binding buffer (1x Tris-Buffered Saline, pH 7.4) and loaded onto a column
561 containing Protein A Agarose beads. The diluted plasma was passed through the column twice, and beads were
562 washed with 1x TBS (20-fold column volume). The bound IgG was eluted with 0.1 M glycine-HCl (pH 2.7), into
563 the neutralizing buffer (1 M Tris-HCl, pH 9.0) and concentrated, and the buffer exchanged into PBS using a 30
564 kDa Amicon Ultra centrifugal filter (Millipore, USA).

565 **Cellulose binding assay using WT and Mutant Luke-2 and Leo-A**

566 To check the cellulose binding activity of WT and mutant Luke-2 and Leo-A, we performed an *in vitro* cellulose
567 binding assay. In this assay, recombinant purified MBP fusion Luke-2 (WT and Ala mutant) and Leo-A (WT and
568 Ala mutant) proteins were used. A total of 1 µg MBP-fusion protein (in 100 µl of 1% NP40) was incubated with
569 0.5 µg Avicel microcrystalline cellulose (Sigma-Aldrich) for 3 hours at 4ºC with rocking. Following binding,
570 microcrystalline cellulose fibers were pelleted down by centrifugation, while the supernatant was collected in a
571 separate tube (unbound fraction). The microcrystalline cellulose fibers (bound fractions) were washed three
572 times with 1% NP40. The input material (total) unbound (U), and bound (B) fractions were boiled in the SDS
573 sample buffer. Soluble proteins were separated on SDS-PAGE (4-15%), blotted to nitrocellulose membranes,
574 blocked in 5% BSA, and detected using anti-MBP antibodies (New England Biolabs). As a negative control,
575 microcrystalline beads were incubated with MBP alone.

576 **Detection of candidate cyst wall lectins in *A. castellanii* trophozoites and cysts**

577 To detect the cyst wall proteins in Ac, log-phase trophozoites parasites and 120 h post-encysting mature cysts
578 were harvested and lysed in SDS sample buffer. The lysates were separated on SDS-PAGE gel (4-15%),
579 transferred on nitrocellulose membrane, and blocked in 5% BSA in PBS. The blots were probed with primary
580 rabbit polyclonal antibodies (1:5000)/purified rabbit IgG (1:1000) raised against the different abundant cyst wall
581 proteins. Anti-rabbit HRP conjugated IgG (Thermo Fisher Scientific) was used as the secondary antibody. Rabbit
582 pre-immune serum or anti-rabbit IgG were used as control. Super Signal West Pico PLUS (Thermo Fisher
583 Scientific) substrate was used for chemiluminescent detection. Blots were imaged using GE ImageQuant LAS
584 4000 gel imager.

585 **Immuno-staining of the mature cysts with purified rabbit polyclonal antibodies**

586 To check the applicability of custom raised polyclonal rabbit antibodies against detection of Jonah-1, Luke-2,
587 Leo-A, and laccase paralogs, we performed IFA imaging using mature cysts from other *Acanthamoeba*
588 species/strains. For IFA imaging, ~0.5 to 1.0 x 10^7 mature cysts (120 h post encystation) from different strains
589 of *Acanthamoeba* were washed in PBS and fixed in 4% paraformaldehyde for 15 minutes at room temperature.
590 Following fixation, cysts were washed three times with PBS and blocked with 1% BSA for 1 h at room
591 temperature. The cysts were further incubated with the rabbit polyclonal antibody (1:200 dilution) for 1h at room
592 temperature. Subsequently these cysts were washed three times with PBS and incubated with secondary anti-
593 rabbit IgG conjugated with Alexa flour 488 (1:300) and Calcofluor White 1:20 (CFW, 1 mg/ml, Sigma Aldrich) for
594 30 min at room temperature. The cysts were washed 3 times with 1x PBS and mounted in VECTASHIELD®
595 Antifade Mounting Medium (Vector Laboratories, Newark, CA). Samples were illuminated using 380nm (CFW),
596 and 488 nm (Alexa flour 488) laser excitation. The stained cysts were imaged using confocal microscope as
597 detailed above. For each rAb and each *Acanthamoeba* isolate, we counted at least 100 cysts in random fields
598 to determine what percentage of CFW-labeled cysts were detected with the rAb. This experiment was repeated
599 twice and counts for the two experiments were averaged. Finally, we examined the same set of slides using a
600 Plan-APO Chromat 100x oil immersion lens on a Zeiss Axio Observer Z1 microscope equipped with Axio Cam
601 ERc5s to show that a confocal microscope was not needed to detect rAb-labeled cysts.
602

603

604 **Figure legends.**

605 **Fig 1. Localization and structure of Jonah lectins. (A)** Drawings show Jonah-1 contains a signal peptide
606 (purple), followed by a Thr-rich spacer (light blue), and a single BHF (green). Jonah-3-AmoebaDB has twelve
607 TMHs (red) and three BHFs, while Jonah-3(c) has three BHFs, three Ser-rich domains (yellow), and no TMHs.
608 **(B)** Confocal microscopy shows Jonah-1 localizes to the ectocyst layer (yellow arrows, stained with WGA). The
609 endocyst layer is marked with CFW (pink arrow), while ostioles appear as dimples (purple arrows). **(C)** Jonah-3-
610 AmoebaDB with 12 TMHs forms rings around ostioles (green arrows) when expressed under its own promoter
611 with a GFP tag. **(D)** Jonah-3(c) localizes to the ectocyst layer, like Jonah-1. Confocal micrographs here and in
612 Fig 2 to 7 were shot with a 60x objective, and 3D reconstructions were made from 0.1 μm optical sections. **(E)**
613 AlphaFold structure with confidence colored shows the Jonah-1 lectin is composed of a single three-sided, β-
614 helical fold (BHF), as well as two α-helices (function unknown), and a 170-aa, unstructured domain rich in Thr
615 (light blue). **(F)** Jonah-3-(c) has three BHFs (red, blue, and yellow) and 132-aa, 267-aa and 308-aa long,
616 unstructured domains rich in Ser (yellow). **(G)** End-view with confidence colored shows the Jonah-1 BHF is three-
617 sided (BHFs may also be two-sided). **(H)** Foldseek analysis shows the Jonah-1 BHF (white) closely matches the
618 BHF of *Colwella sp.* (blue), the structure of which has been solved (PDB 3WP9). The E-value is 5.10e-4, and
619 the RMSD is 9.21, despite a sequence identity of just 12% over a 245-aa overlap. Scale bars for **B** to **D** are each
620 5 μm.

621 **Fig 2. Structure and localization and structure of Luke-2.** A. Drawings show Luke-2 and Luke-3 contain a
622 signal peptide (purple) and two or three β-jelly roll folds (BJRFs) (orange), respectively, which are separated by
623 Ser-rich spacers (yellow). B. Confocal microscopy shows WT Luke-2-GFP localizes to the endocyst layer (pink
624 arrows) and forms a flat ring around ostioles (blue-green arrows) (see also Fig. 5D). C. When five Tyr and a Phe
625 are mutated to Ala (see H and I below), Ala-mut Luke-2-GFP no longer localizes to endocyst layer. D. AlphaFold
626 shows Luke-2 contains two BJRFs, which are separated by a 47-aa unstructured, spacer rich in Ser (yellow). E.
627 Luke-3 has three BHFs separated by 42-aa and 33-aa long, unstructured spacers that are also Ser-rich. F and
628 G. Foldseek shows the N-half BJRF of Luke-2 shares a similar structure with a BJRF of *Dictyostelium* wall protein
629 and with CBM2 of a *Cellulomonas fimi* endoglucanase (blue), the structure of which has been solved (PDB

630 1EXH). The E-value for the BJRFs of Luke-2 and *D. discoideum* wall protein is 4.99e-7, and the RMSD is 1.79,
631 strongly suggesting common ancestry. The E-value for the N-terminal BJRF of Luke-2 and the CBM2 of *C. fimi*
632 is 9.72e-5, and the RMSD is 5.01, despite a 16% identity over a 105-aa overlap. The N-terminal BJRF of Luke-
633 2 has three linearly arranged aromatics (orange), which match those of *D. discoideum* and *C. fimi* (pink arrows).
634 H and I. Surface views of Luke-2-N and Luke-2-C highlight linear arrays of Trp (blue) and Phe (pink), which were
635 mutated to make Ala-mut of Luke-2-GFP that no longer localizes to the endocyst layer and ostioles (see B
636 above). J. Western blots show that MBP alone fails to bind to Avicel cellulose, while MBP-Luke-2 and MBP-
637 Leo-A fusion-proteins (described in Fig. 3) each bind well to Avicel cellulose. In contrast, cellulose binding is lost
638 when six aromatics are mutated to Ala in both Luke-2 and Leo-A. These experiments support the idea that Ala-
639 mutants of Leo-A and Luke-2 mislocalize in cyst walls, because of the loss of cellulose binding. Scale bars for **B**
640 and **C** are each 5 μm.

641 **Fig 3. Structure and localization of Leo lectins. (A)** Drawings show Leo-A contains a signal peptide (purple)
642 and two adjacent sets of four disulfide knots (4DKs) (blue), while Leo-S contains a Thr-rich spacer (grey-blue)
643 between sets of 4DKs. **(B)** Confocal microscopy shows WT Leo-A localizes to the endocyst layer (pink arrows)
644 and forms a flat ring around ostioles (blue-green arrows) (see also Fig 5D). **(C)**. When six Tyr are mutated to Ala
645 (see H below), Ala-mut Leo-A (grey arrow) no longer localizes to endocyst layer. **(D)** Early in encystation (12
646 hours), secretory vesicles (SV) containing Leo-S(c) fill the cytosol of Ac, which lack a cyst wall as shown by
647 failure to label with WGA or CFW. **(E)** Later in encystation (24 hours), Leo-S(c) has a somewhat patchy
648 distribution in the single-layered wall, which now labels with WGA and CFW. **(F)** In mature cyst walls (72 hours),
649 Leo-S(c) has a homogeneous distribution in the ectocyst layer (yellow arrows). Note that CFW predominantly
650 labels the endocyst layer of mature cysts. **(G)** A ribbon diagram of Leo-A highlights 4DKs (red spheres), which
651 connect short, parallel loops. **(H)** The surface of Leo-A shows three Tyr residues (green) linearly arrayed in each
652 4DK, which were mutated to Ala to test the effects on localization (see C above) and cellulose-binding (see Fig
653 2J). **(I)** The surface of Leo-S-corrected shows a 252-aa long unstructured, spacer rich in Thr (blue) between
654 4DKs, each of which contains linearly arrayed Tyr residues. Foldseek had no hit with the structure of Leo-A.
655 Scale bars for **B** to **F** are each 5 μm.

656

657 **Fig 4. Localization and structure of an abundant laccase. (A)** The Ac Laccase-1 has signal peptide (purple)
658 and three copper oxidase domains (red), separated by short, unstructured spacers lacking either Ser- or Thr
659 (white). **(B)** Confocal microscopy shows that early in encystation (18 hours) secretory vesicles (SV) containing
660 laccase-GFP fill the cytosol of Ac, which lack a cyst wall as shown by failure to label with WGA or CFW. **(C)** Later
661 in encystation (24 hours), laccase-GFP has a homogeneous distribution in the single-layered wall, which now
662 labels with lightly with WGA and somewhat more with CFW. **(D)** In mature cyst walls (72 hours), laccase-GFP
663 has the same homogeneous distribution in the ectocyst layer (yellow arrows) with ostioles as dimples (purple
664 arrows). **(E)** AlphaFold structure shows CuRO-1 (blue), CuRO-2 (red), and CuRO-3 (yellow) domains of the
665 laccase, all of which are predicted with confidence (not shown). **(G)** Typical for an enzyme, the E-value is 1.32e-
666 59 and the RMSD = 2.75 with a sequence identity of 39% over a 505-aa overlap. Scale bars for **B** to **D** are each
667 5 μm.
668 **Fig 5. Promoter swaps between either Jonah-1 and Luke-2 or laccase-1 and Leo-A. (A)** RT-PCR shows
669 that ectocyst proteins (Jonah-1 and laccase-1) are made earlier than endocyst proteins (Luke-2 and Leo-A).
670 Note values for each time points are normalized with calreticulin, which is highly expressed in trophozoites and
671 encysting Ac. **(B)** In the first promoter swap, Jonah-1-GFP expressed under its own earlier promoter localizes to
672 the ectocyst layer (yellow arrow) (see also Fig 1B). **(C)** Expression under the later Luke-2 promoter causes
673 Jonah-1-GFP to localize to the ostioles (blue-green arrows), which increase in thickness and number, while there
674 is minimal localization of Jonah-1-GFP to the endocyst layer (pink arrows). **(D)** Conversely, Luke-2-GFP under
675 its own later promoter localizes to the endocyst layer and forms a narrow ring around ostioles (see also Fig 2B)
676 **(E)** Expression under the earlier Jonah-1 promoter causes Luke-2 to relocate to the ectocyst layer. Remarkably,
677 the narrow ring of Luke-2-GFP around the ostioles appears the same under either its own or the Jonah-1
678 promoter, suggesting its target glycopolymer is available early and later during encystation. **(F)** In the second
679 promoter swap, laccase-1-GFP expressed under its own earlier promoter localizes to the ectocyst layer (see
680 also Fig 4D). **(G)** Expression under the later Leo-A promoter causes laccase-1-GFP to localize to the ostioles
681 with minimal localization to the endocyst layer. **(H)** Conversely, Leo-A-GFP under its own later promoter localizes
682 to the endocyst layer and forms a narrow ring around ostioles. **(I)** Expression under the earlier laccase promoter
683 causes Leo-A to localize to the ectocyst layer and forms a narrow ring around ostioles. These experiments show

684 that under both early and late promoters, Jonah-1 and Laccase-1 have similar localizations in the cyst wall,
685 suggesting that each bind to the same glycopolymer(s). Luke-2 and Leo-A also have similar localizations under
686 early and late promoters, but the localization is distinct from that of Jonah-1 and Laccase-1, suggesting pairs of
687 wall proteins are binding to different glycopolymers. Scale bars for **B** to **I** are each 5 µm.

688 **Fig. 6. Binding of rAbs to cyst wall proteins and to Neff strain Ac. (A)** Western blots show pre-bleeds from
689 rabbits (negative control) fail to bind to proteins of trophozoites or cysts, while rAbs fail to bind to trophozoite
690 proteins (a second negative control) but bind well to cyst proteins of Neff strain. As discussed in detail in the
691 Results, rAbs to the BHF of Jonah-1 binds to the expected 55-kDa band and to two lower mol wt bands. Anti-
692 Luke-2 rAbs bind to a heavy and broad 50-kDa band, which is greater than the expected size of 27-kDa. Anti-
693 Leo rAbs bind to a 13-kDa band, which is slightly smaller than the expected size of 17-kDA. Anti-laccase rAbs
694 bind to a 75-kDa band, which is slightly bigger than the expected size of 64-kDa, as well as to a less abundant
695 55-kDa band. **(B)** High power confocal microscopy shows rAbs to Jonah-1 bind in a patchy distribution to the
696 surface of Neff strain of Ac and other *Acanthamoeba* species, which are shown in Fig 7A. **(C)** Anti-Luke-2 rAbs
697 bind strongly to ostioles and weakly to endocyst layer of some but not all Neff strain Ac. An asterisk is attached
698 to "ostioles" because anti-Luke-2 rAbs can also bind to ectocyst layer, as shown in Fig 7B. **(D)** Anti-Leo-A rAbs
699 also bind strongly to ostioles with a variable binding to the endocyst layer of some but not all of Neff strain Ac.
700 Again, an asterisk indicates that anti-Leo-A rAbs can also bind to the ectocyst layer, as shown in Fig 7C. **(E)**
701 Anti-laccase-1 rAbs bind in a homogenous manner to cysts of Neff strain, as well as to cyst of other
702 Acanthamoeba species, which are shown in Fig 7D. **(F to I)**. Low power confocal micrographs shows rAbs to
703 Jonah-1, Luke-2, Leo-A and laccase-1 detect well CFW-labeled cysts of the Neff strain. **(J)** A plot shows the
704 percentage of CFW-labeled cysts detected by four rAbs in two independent experiments (average plus SEM), in
705 which 100+ cysts were counted in random low power fields. Rabbit antibodies to Luke-2, Leo-A, and Laccase-1
706 each detect >95% of cysts 10 of 11 *Acanthamoeba* isolates tested, while rAbs to Jonah-1 are slightly less
707 efficient in detecting three isolates of *Acanthamoeba*. The exception is *A. mauritaniensis*, which was poorly
708 detected with all four rAbs, suggesting a problem with cyst formation under the conditions used here. Single
709 scale bar for **B** to **E** is 5 µm.

710 **Fig 7. Binding of rAbs to Jonah-1, Luke-2, Leo-A, and Laccase to a diverse set of *Acanthamoeba Spp.***
711 **cysts**. High power confocal micrographs show binding of rAbs to cysts ten *Acanthamoeba* isolates, the identities
712 of which were confirmed by sequencing 18S RNAs. Column **(A)** Anti-Jonah-1 rAbs bind in a patchy distribution
713 to the ectocyst layer (surface) of most cysts of *Acanthamoeba* isolates. Column **(B)** Anti-Luke-2 rAbs bind to the
714 endocyst layer and ostioles of some cysts (e.g., *A. polyphaga, A. hatchetii, A, byersi*, and ESBC4) and to the
715 ectocyst layer of other cysts (e.g., three *A. castellanii* and *A. astronyxis*). Asterisks indicate heterogeneous
716 distribution of rAbs among the same *Acanthamoeba* isolate. Column **(C)** Anti-Leo-A rAbs also have a
717 heterogeneous distribution on the ectocyst layer, endocyst layer, and/or ostioles. In some cases anti-Leo-A
718 distribution matches that of anti-Luke-2 (e.g., *A. astronyxis, A. byersi*, and *A. sp. 13*), in the same way that Leo-
719 GFP and Luke-GFP match in the promoter swap experiments (Fig 5). Column **(D)** Anti-Jonah-1 rAbs bind in a
720 homogeneous distribution to the ectocyst layer (surface) of the vast majority of cysts of *Acanthamoeba* isolates.
721 Counts of CFW-labeled cysts by each antibody are shown in Fig 6J. Single scale bar for **A** to **D** is 50 μm.

722 **Acknowledgments**

723 Thanks to Jonathan Stefely (Massachusetts General Hospital), Sarah Calvo (Broad Institute and Howard Hughes
724 Medical Institute), and Brian Haas (Broad Institute) for access to the unfinished transcriptome analysis
725 of *Acanthamoeba castellanii* Neff strain. Thanks to Monica Crary of Alcon, Inc. and Noorjahan Panjwani of Tufts
726 University for cultures of *Acanthamoeba*. Thanks to Cataldo Leone, Dean of BUSDM for financial support for this
727 work. This paper is dedicated to Jude, the cousin of Jonah, Luke, and Leo.

728

729 Supporting Information S1 lists the primers used for making constructs and for performing qRT-PCR.
730 Supporting Information S2 lists promoter sequences and coding sequences of the abundant cyst wall proteins
731 used for making GFP-tagged proteins. Also listed are the coding sequences used to make MBP-fusions for
732 testing cellulose binding and for immunizing rabbits.

References

1. Azzopardi M, Chong YJ, Ng B, Recchioni A, Logeswaran A, Ting DSJ. Diagnosis of Acanthamoeba Keratitis: Past, Present and Future. Diagnostics (Basel). 2023;13(16). Epub 2023/08/26. doi: 10.3390/diagnostics13162655. PubMed PMID: 37627913; PubMed Central PMCID: PMCPMC10453105.
2. Bouten M EH. Diagnosis and Management of Acanthamoeba Keratitis: A Continental Approach. Parasitologia. 2022;2:167-97.
3. Carnt N, Hoffman JM, Verma S, Hau S, Radford CF, Minassian DC, et al. Acanthamoeba keratitis: confirmation of the UK outbreak and a prospective case-control study identifying contributing risk factors. Br J Ophthalmol. 2018;102(12):1621-8. Epub 2018/09/21. doi: 10.1136/bjophthalmol-2018-312544. PubMed PMID: 30232172.
4. Satlin MJ, Graham JK, Visvesvara GS, Mena H, Marks KM, Saal SD, et al. Fulminant and fatal encephalitis caused by Acanthamoeba in a kidney transplant recipient: case report and literature review. Transpl Infect Dis. 2013;15(6):619-26. Epub 2013/09/10. doi: 10.1111/tid.12131. PubMed PMID: 24010955.
5. Dos Santos DL, Kwitko S, Marinho DR, de Araujo BS, Locatelli CI, Rott MB. Acanthamoeba keratitis in Porto Alegre (southern Brazil): 28 cases and risk factors. Parasitol Res. 2018;117(3):747-50. Epub 2018/01/15. doi: 10.1007/s00436-017-5745-y. PubMed PMID: 29332157.
6. Ghaderifar S, Najafpoor AA, Zarrinfar H, Esmaily H, Hajialilo E. Isolation and identification of Acanthamoeba from pond water of parks in a tropical and subtropical region in the Middle East, and its relation with physicochemical parameters. BMC Microbiol. 2018;18(1):139. Epub 2018/10/21. doi: 10.1186/s12866-018-1301-x. PubMed PMID: 30340522; PubMed Central PMCID: PMCPMC6195741.
7. Henriquez FL, Campbell SJ, Sundararaj BK, Cano A, Muench SP, Roberts CW. The Acanthamoeba shikimate pathway has a unique molecular arrangement and is essential for aromatic amino acid biosynthesis. Protist. 2015;166(1):93-105. Epub 2015/01/13. doi: 10.1016/j.protis.2014.12.001. PubMed PMID: 25576842.
8. Pittet D, Allegranzi B, Boyce J, World Health Organization World Alliance for Patient Safety First Global Patient Safety Challenge Core Group of E. The World Health Organization Guidelines on Hand Hygiene in Health Care and their consensus recommendations. Infect Control Hosp Epidemiol. 2009;30(7):611-22. Epub 2009/06/11. doi: 10.1086/600379. PubMed PMID: 19508124.
9. Zhang Y, Xu X, Wei Z, Cao K, Zhang Z, Liang Q. The global epidemiology and clinical diagnosis of Acanthamoeba keratitis. J Infect Public Health. 2023;16(6):841-52. Epub 2023/04/09. doi: 10.1016/j.jiph.2023.03.020. PubMed PMID: 37030037.
10. Brown AC, Ross J, Jones DB, Collier SA, Ayers TL, Hoekstra RM, et al. Risk Factors for Acanthamoeba Keratitis-A Multistate Case-Control Study, 2008-2011. Eye Contact Lens. 2018;44 Suppl 1:S173-S8. Epub 2017/01/19. doi: 10.1097/ICL.0000000000000365. PubMed PMID: 28099282.
11. Carnt N, Robaei D, Minassian DC, Dart JKG. Acanthamoeba keratitis in 194 patients: risk factors for bad outcomes and severe inflammatory complications. Br J Ophthalmol. 2018;102(10):1431-5. Epub 2018/01/05. doi: 10.1136/bjophthalmol-2017-310806. PubMed PMID: 29298778.
12. Lorenzo-Morales J, Martin-Navarro CM, Lopez-Arencibia A, Arnalich-Montiel F, Pinero JE, Valladares B. Acanthamoeba keratitis: an emerging disease gathering importance worldwide? Trends Parasitol. 2013;29(4):181-7. Epub 2013/02/26. doi: 10.1016/j.pt.2013.01.006. PubMed PMID: 23433689.
13. Diehl MLN, Paes J, Rott MB. Genotype distribution of Acanthamoeba in keratitis: a systematic review. Parasitol Res. 2021;120(9):3051-63. Epub 2021/08/06. doi: 10.1007/s00436-021-07261-1. PubMed PMID: 34351492; PubMed Central PMCID: PMCPMC8339388.
14. Fuerst PA. The Status of Molecular Analyses of Isolates of Acanthamoeba Maintained by International Culture Collections. Microorganisms. 2023;11(2). Epub 2023/02/26. doi: 10.3390/microorganisms11020295. PubMed PMID: 36838260; PubMed Central PMCID: PMCPMC9961329.

15. Fuerst PA, Booton GC, Crary M. Phylogenetic analysis and the evolution of the 18S rRNA gene typing system of Acanthamoeba. J Eukaryot Microbiol. 2015;62(1):69-84. Epub 2014/10/07. doi: 10.1111/jeu.12186. PubMed PMID: 25284310.
16. Rayamajhee B, Sharma S, Willcox M, Henriquez FL, Rajagopal RN, Shrestha GS, et al. Assessment of genotypes, endosymbionts and clinical characteristics of Acanthamoeba recovered from ocular infection. BMC Infect Dis. 2022;22(1):757. Epub 2022/09/30. doi: 10.1186/s12879-022-07741-4. PubMed PMID: 36175838; PubMed Central PMCID: PMCPMC9520893.
17. Amos B, Aurrecoechea C, Barba M, Barreto A, Basenko EY, Bazant W, et al. VEuPathDB: the eukaryotic pathogen, vector and host bioinformatics resource center. Nucleic Acids Res. 2022;50(D1):D898-D911. Epub 2021/11/01. doi: 10.1093/nar/gkab929. PubMed PMID: 34718728; PubMed Central PMCID: PMCPMC8728164.
18. Clarke M, Lohan AJ, Liu B, Lagkouvardos I, Roy S, Zafar N, et al. Genome of Acanthamoeba castellanii highlights extensive lateral gene transfer and early evolution of tyrosine kinase signaling. Genome Biol. 2013;14(2):R11. Epub 2013/02/05. doi: 10.1186/gb-2013-14-2-r11. PubMed PMID: 23375108; PubMed Central PMCID: PMCPMC4053784.
19. Bernard C, Locard-Paulet M, Noel C, Duchateau M, Giai Gianetto Q, Moumen B, et al. A time-resolved multi-omics atlas of Acanthamoeba castellanii encystment. Nat Commun. 2022;13(1):4104. Epub 2022/07/15. doi: 10.1038/s41467-022-31832-0. PubMed PMID: 35835784; PubMed Central PMCID: PMCPMC9283445.
20. Matthey-Doret C, Colp MJ, Escoll P, Thierry A, Moreau P, Curtis B, et al. Chromosome-scale assemblies of Acanthamoeba castellanii genomes provide insights into Legionella pneumophila infection-related chromatin reorganization. Genome Res. 2022;32(9):1698-710. Epub 2022/09/16. doi: 10.1101/gr.276375.121. PubMed PMID: 36109147; PubMed Central PMCID: PMCPMC9528979.
21. Jensen T, Barnes WG, Meyers D. Axenic cultivation of large populations of Acanthamoeba castellanii (JBM). J Parasitol. 1970;56(5):904-6. Epub 1970/10/01. PubMed PMID: 5504530.
22. Neff RJ, Ray SA, Benton WF, Wilborn M. Induction of synchronous encystment (differentiation) in Acanthamoeba spp. Methods in Cell Biology. 1964;1:55-83. doi:10.1016/S0091-679X(08)62086-5.
23. Aqeel Y, Rodriguez R, Chatterjee A, Ingalls RR, Samuelson J. Killing of diverse eye pathogens (Acanthamoeba spp., Fusarium solani, and Chlamydia trachomatis) with alcohols. PLoS Negl Trop Dis. 2017;11(2):e0005382. Epub 2017/02/10. doi: 10.1371/journal.pntd.0005382. PubMed PMID: 28182670; PubMed Central PMCID: PMCPMC5321442.
24. Campolo A, Pifer R, Walters R, Thomas M, Miller E, Harris V, et al. Acanthamoeba spp. aggregate and encyst on contact lens material increasing resistance to disinfection. Front Microbiol. 2022;13:1089092. Epub 2023/01/06. doi: 10.3389/fmicb.2022.1089092. PubMed PMID: 36601401; PubMed Central PMCID: PMCPMC9806144.
25. Coulon C, Collignon A, McDonnell G, Thomas V. Resistance of Acanthamoeba cysts to disinfection treatments used in health care settings. J Clin Microbiol. 2010;48(8):2689-97. Epub 2010/06/04. doi: 10.1128/JCM.00309-10. PubMed PMID: 20519477; PubMed Central PMCID: PMCPMC2916629.
26. Dupuy M, Berne F, Herbelin P, Binet M, Berthelot N, Rodier MH, et al. Sensitivity of free-living amoeba trophozoites and cysts to water disinfectants. Int J Hyg Environ Health. 2014;217(2-3):335-9. Epub 2013/08/13. doi: 10.1016/j.ijheh.2013.07.007. PubMed PMID: 23932411.
27. Walters R, Campolo A, Miller E, McAnally C, Gabriel M, Shannon P, et al. Differential Antimicrobial Efficacy of Preservative-Free Contact Lens Disinfection Systems against Common Ocular Pathogens. Microbiol Spectr. 2022;10(1):e0213821. Epub 2022/02/10. doi: 10.1128/spectrum.02138-21. PubMed PMID: 35138157; PubMed Central PMCID: PMCPMC8826922.
28. Wang Y, Jiang L, Zhao Y, Ju X, Wang L, Jin L, et al. Biological characteristics and pathogenicity of Acanthamoeba. Front Microbiol. 2023;14:1147077. Epub 2023/04/24. doi: 10.3389/fmicb.2023.1147077. PubMed PMID: 37089530; PubMed Central PMCID: PMCPMC10113681.

826 29. Magistrado-Coxen P, Aqeel Y, Lopez A, Haserick JR, Urbanowicz BR, Costello CE, et al. The most
827 abundant cyst wall proteins of Acanthamoeba castellanii are lectins that bind cellulose and localize to distinct
828 structures in developing and mature cyst walls. PLoS Negl Trop Dis. 2019;13(5):e0007352. Epub 2019/05/17.
829 doi: 10.1371/journal.pntd.0007352. PubMed PMID: 31095564; PubMed Central PMCID: PMCPMC6541295.
830 30. Wilhelmus KR, Osato MS, Font RL, Robinson NM, Jones DB. Rapid diagnosis of Acanthamoeba keratitis
831 using calcofluor white. Arch Ophthalmol. 1986;104(9):1309-12. Epub 1986/09/01. doi:
832 10.1001/archopht.1986.01050210063026. PubMed PMID: 2428343.
833 31. Orlean P. Architecture and biosynthesis of the Saccharomyces cerevisiae cell wall. Genetics.
834 2012;192(3):775-818. Epub 2012/11/09. doi: 10.1534/genetics.112.144485. PubMed PMID: 23135325;
835 PubMed Central PMCID: PMCPMC3522159.
836 32. West CM. Comparative analysis of spore coat formation, structure, and function in Dictyostelium. Int
837 Rev Cytol. 2003;222:237-93. Epub 2002/12/31. doi: 10.1016/s0074-7696(02)22016-1. PubMed PMID:
838 12503851.
839 33. Zablackis E, Huang J, Muller B, Darvill AG, Albersheim P. Characterization of the cell-wall
840 polysaccharides of Arabidopsis thaliana leaves. Plant Physiol. 1995;107(4):1129-38. Epub 1995/04/01. doi:
841 10.1104/pp.107.4.1129. PubMed PMID: 7770522; PubMed Central PMCID: PMCPMC157245.
842 34. Bowers B, Korn ED. The fine structure of Acanthamoeba castellanii (Neff strain). II. Encystment. J Cell
843 Biol. 1969;41(3):786-805. Epub 1969/06/01. doi: 10.1083/jcb.41.3.786. PubMed PMID: 5768875; PubMed
844 Central PMCID: PMCPMC2107820.
845 35. Potter JL, Weisman RA. Cellulose synthesis by extracts of Acanthamoeba castellanii during encystment.
846 Stimulation of the incorporation of radioactivity from UDP-(14C)glucose into alkali-soluble and insoluble beta-
847 glucans by glucose 6-phosphate and related compounds. Biochim Biophys Acta. 1976;428(1):240-52. Epub
848 1976/03/25. doi: 10.1016/0304-4165(76)90125-2. PubMed PMID: 1260020.
849 36. Morozov AA, Likhoshway YV. Evolutionary history of the chitin synthases of eukaryotes. Glycobiology.
850 2016;26(6):635-9. Epub 2016/02/19. doi: 10.1093/glycob/cww018. PubMed PMID: 26887391.
851 37. Bateman E. Expression plasmids and production of EGFP in stably transfected Acanthamoeba. Protein
852 Expr Purif. 2010;70(1):95-100. Epub 2009/10/20. doi: 10.1016/j.pep.2009.10.008. PubMed PMID: 19836453;
853 PubMed Central PMCID: PMCPMC2822096.
854 38. Peng Z, Omaruddin R, Bateman E. Stable transfection of Acanthamoeba castellanii. Biochim Biophys
855 Acta. 2005;1743(1-2):93-100. Epub 2005/03/22. doi: 10.1016/j.bbamcr.2004.08.014. PubMed PMID:
856 15777844.
857 39. Jumper J, Evans R, Pritzel A, Green T, Figurnov M, Ronneberger O, et al. Highly accurate protein
858 structure prediction with AlphaFold. Nature. 2021;596(7873):583-9. Epub 2021/07/16. doi: 10.1038/s41586-
859 021-03819-2. PubMed PMID: 34265844; PubMed Central PMCID: PMCPMC8371605 have filed non-provisional
860 patent applications 16/701,070 and PCT/EP2020/084238, and provisional patent applications 63/107,362,
861 63/118,917, 63/118,918, 63/118,921 and 63/118,919, each in the name of DeepMind Technologies Limited,
862 each pending, relating to machine learning for predicting protein structures. The other authors declare no
863 competing interests.
864 40. van Kempen M, Kim SS, Tumescheit C, Mirdita M, Lee J, Gilchrist CLM, et al. Fast and accurate protein
865 structure search with Foldseek. Nat Biotechnol. 2023. Epub 2023/05/09. doi: 10.1038/s41587-023-01773-0.
866 PubMed PMID: 37156916.
867 41. Varadi M, Anyango S, Deshpande M, Nair S, Natassia C, Yordanova G, et al. AlphaFold Protein Structure
868 Database: massively expanding the structural coverage of protein-sequence space with high-accuracy models.
869 Nucleic Acids Res. 2022;50(D1):D439-D44. Epub 2021/11/19. doi: 10.1093/nar/gkab1061. PubMed PMID:
870 34791371; PubMed Central PMCID: PMCPMC8728224.

871 42. Boraston AB, Bolam DN, Gilbert HJ, Davies GJ. Carbohydrate-binding modules: fine-tuning
872 polysaccharide recognition. Biochem J. 2004;382(Pt 3):769-81. Epub 2004/06/25. doi: 10.1042/BJ20040892.
873 PubMed PMID: 15214846; PubMed Central PMCID: PMCPMC1133952.
874 43. Consortium CA. Ten years of CAZypedia: a living encyclopedia of carbohydrate-active enzymes.
875 Glycobiology. 2018;28(1):3-8. Epub 2017/10/19. doi: 10.1093/glycob/cwx089. PubMed PMID: 29040563.
876 44. Cosgrove DJ. Microbial Expansins. Annu Rev Microbiol. 2017;71:479-97. Epub 2017/09/10. doi:
877 10.1146/annurev-micro-090816-093315. PubMed PMID: 28886679.
878 45. Gilbert HJ, Knox JP, Boraston AB. Advances in understanding the molecular basis of plant cell wall
879 polysaccharide recognition by carbohydrate-binding modules. Curr Opin Struct Biol. 2013;23(5):669-77. Epub
880 2013/06/19. doi: 10.1016/j.sbi.2013.05.005. PubMed PMID: 23769966.
881 46. Lombard V, Golaconda Ramulu H, Drula E, Coutinho PM, Henrissat B. The carbohydrate-active enzymes
882 database (CAZy) in 2013. Nucleic Acids Res. 2014;42(Database issue):D490-5. Epub 2013/11/26. doi:
883 10.1093/nar/gkt1178. PubMed PMID: 24270786; PubMed Central PMCID: PMCPMC3965031.
884 47. Urbanowicz BR, Catala C, Irwin D, Wilson DB, Ripoll DR, Rose JK. A tomato endo-beta-1,4-glucanase,
885 SlCel9C1, represents a distinct subclass with a new family of carbohydrate binding modules (CBM49). J Biol
886 Chem. 2007;282(16):12066-74. Epub 2007/02/27. doi: 10.1074/jbc.M607925200. PubMed PMID: 17322304.
887 48. Hallgren J. TKD, Pedersen M.D., Almagro Armenteros J.J., Marcatili P., Nielsen H., Krogh A., Winther O.
888 DeepTMHMM predicts alpha and beta transmembrane proteins using deep neural networks. bioRxiv. 2022.
889 doi: doi: 10.1101/2022.04.08.487609.
890 49. Nielsen H. Predicting Secretory Proteins with SignalP. Methods Mol Biol. 2017;1611:59-73. Epub
891 2017/04/30. doi: 10.1007/978-1-4939-7015-5_6. PubMed PMID: 28451972.
892 50. Enguita FJ, Martins LO, Henriques AO, Carrondo MA. Crystal structure of a bacterial endospore coat
893 component. A laccase with enhanced thermostability properties. J Biol Chem. 2003;278(21):19416-25. Epub
894 2003/03/15. doi: 10.1074/jbc.M301251200. PubMed PMID: 12637519.
895 51. Kiiskinen LL, Palonen H, Linder M, Viikari L, Kruus K. Laccase from Melanocarpus albomyces binds
896 effectively to cellulose. FEBS Lett. 2004;576(1-2):251-5. Epub 2004/10/12. doi: 10.1016/j.febslet.2004.08.040.
897 PubMed PMID: 15474046.
898 52. Banerjee S, Vishwanath P, Cui J, Kelleher DJ, Gilmore R, Robbins PW, et al. The evolution of N-glycan-
899 dependent endoplasmic reticulum quality control factors for glycoprotein folding and degradation. Proc Natl
900 Acad Sci U S A. 2007;104(28):11676-81. Epub 2007/07/04. doi: 10.1073/pnas.0704862104. PubMed PMID:
901 17606910; PubMed Central PMCID: PMCPMC1905923.
902 53. Altschul SF, Madden TL, Schaffer AA, Zhang J, Zhang Z, Miller W, et al. Gapped BLAST and PSI-BLAST: a
903 new generation of protein database search programs. Nucleic Acids Res. 1997;25(17):3389-402. Epub
904 1997/09/01. doi: 10.1093/nar/25.17.3389. PubMed PMID: 9254694; PubMed Central PMCID:
905 PMCPMC146917.
906 54. Finn RD, Attwood TK, Babbitt PC, Bateman A, Bork P, Bridge AJ, et al. InterPro in 2017-beyond protein
907 family and domain annotations. Nucleic Acids Res. 2017;45(D1):D190-D9. Epub 2016/12/03. doi:
908 10.1093/nar/gkw1107. PubMed PMID: 27899635; PubMed Central PMCID: PMCPMC5210578.
909 55. Wang Y, Slade MB, Gooley AA, Atwell BJ, Williams KL. Cellulose-binding modules from extracellular
910 matrix proteins of Dictyostelium discoideum stalk and sheath. Eur J Biochem. 2001;268(15):4334-45. Epub
911 2001/08/08. doi: 10.1046/j.1432-1327.2001.02354.x. PubMed PMID: 11488929.
912 56. Xu Y, Liang X, Chen Y, Koehler TM, Hook M. Identification and biochemical characterization of two
913 novel collagen binding MSCRAMMs of Bacillus anthracis. J Biol Chem. 2004;279(50):51760-8. Epub
914 2004/10/01. doi: 10.1074/jbc.M406417200. PubMed PMID: 15456768.
915 57. Davies G, Henrissat B. Structures and mechanisms of glycosyl hydrolases. Structure. 1995;3(9):853-9.
916 Epub 1995/09/15. doi: 10.1016/S0969-2126(01)00220-9. PubMed PMID: 8535779.

917 58. Xu GY, Ong E, Gilkes NR, Kilburn DG, Muhandiram DR, Harris-Brandts M, et al. Solution structure of a
918 cellulose-binding domain from Cellulomonas fimi by nuclear magnetic resonance spectroscopy. Biochemistry.
919 1995;34(21):6993-7009. Epub 1995/05/30. PubMed PMID: 7766609.
920 59. Duong-Ly KC, Gabelli SB. Affinity Purification of a Recombinant Protein Expressed as a Fusion with the
921 Maltose-Binding Protein (MBP) Tag. Methods Enzymol. 2015;559:17-26. Epub 2015/06/23. doi:
922 10.1016/bs.mie.2014.11.004. PubMed PMID: 26096500; PubMed Central PMCID: PMCPMC4612625.
923 60. Kapust RB, Waugh DS. Escherichia coli maltose-binding protein is uncommonly effective at promoting
924 the solubility of polypeptides to which it is fused. Protein Sci. 1999;8(8):1668-74. Epub 1999/08/19. doi:
925 10.1110/ps.8.8.1668. PubMed PMID: 10452611; PubMed Central PMCID: PMCPMC2144417.
926 61. Chatterjee A, Ghosh SK, Jang K, Bullitt E, Moore L, Robbins PW, et al. Evidence for a "wattle and daub"
927 model of the cyst wall of entamoeba. PLoS Pathog. 2009;5(7):e1000498. Epub 2009/07/07. doi:
928 10.1371/journal.ppat.1000498. PubMed PMID: 19578434; PubMed Central PMCID: PMCPMC2698119.
929 62. Harata K, Nagahora H, Jigami Y. X-ray structure of wheat germ agglutinin isolectin 3. Acta Crystallogr D
930 Biol Crystallogr. 1995;51(Pt 6):1013-9. Epub 1995/11/01. doi: 10.1107/S0907444995004070. PubMed PMID:
931 15299769.
932 63. Kuranda MJ, Robbins PW. Chitinase is required for cell separation during growth of Saccharomyces
933 cerevisiae. J Biol Chem. 1991;266(29):19758-67. Epub 1991/10/15. PubMed PMID: 1918080.
934 64. Van Dellen K, Ghosh SK, Robbins PW, Loftus B, Samuelson J. Entamoeba histolytica lectins contain
935 unique 6-Cys or 8-Cys chitin-binding domains. Infect Immun. 2002;70(6):3259-63. Epub 2002/05/16. doi:
936 10.1128/IAI.70.6.3259-3263.2002. PubMed PMID: 12011021; PubMed Central PMCID: PMCPMC127964.
937 65. Hanada Y, Nishimiya Y, Miura A, Tsuda S, Kondo H. Hyperactive antifreeze protein from an Antarctic
938 sea ice bacterium Colwellia sp. has a compound ice-binding site without repetitive sequences. FEBS J.
939 2014;281(16):3576-90. Epub 2014/06/19. doi: 10.1111/febs.12878. PubMed PMID: 24938370.
940 66. Liu Z, Xie T, Zhong Q, Wang G. Crystal structure of CotA laccase complexed with 2,2-azinobis-(3-
941 ethylbenzothiazoline-6-sulfonate) at a novel binding site. Acta Crystallogr F Struct Biol Commun. 2016;72(Pt
942 4):328-35. Epub 2016/04/07. doi: 10.1107/S2053230X1600426X. PubMed PMID: 27050268; PubMed Central
943 PMCID: PMCPMC4822991.
944 67. Schiller B, Makrypidi G, Razzazi-Fazeli E, Paschinger K, Walochnik J, Wilson IB. Exploring the unique N-
945 glycome of the opportunistic human pathogen Acanthamoeba. J Biol Chem. 2012;287(52):43191-204. Epub
946 2012/11/10. doi: 10.1074/jbc.M112.418095. PubMed PMID: 23139421; PubMed Central PMCID:
947 PMCPMC3527907.
948 68. Garate M, Cubillos I, Marchant J, Panjwani N. Biochemical characterization and functional studies of
949 Acanthamoeba mannose-binding protein. Infect Immun. 2005;73(9):5775-81. Epub 2005/08/23. doi:
950 10.1128/IAI.73.9.5775-5781.2005. PubMed PMID: 16113295; PubMed Central PMCID: PMCPMC1231072.
951 69. Samuelson J, Bushkin GG, Chatterjee A, Robbins PW. Strategies to discover the structural components
952 of cyst and oocyst walls. Eukaryot Cell. 2013;12(12):1578-87. Epub 2013/10/08. doi: 10.1128/EC.00213-13.
953 PubMed PMID: 24096907; PubMed Central PMCID: PMCPMC3889564.
954 70. Ghosh SK, Van Dellen KL, Chatterjee A, Dey T, Haque R, Robbins PW, et al. The Jacob2 lectin of the
955 Entamoeba histolytica cyst wall binds chitin and is polymorphic. PLoS Negl Trop Dis. 2010;4(7):e750. Epub
956 2010/07/24. doi: 10.1371/journal.pntd.0000750. PubMed PMID: 20652032; PubMed Central PMCID:
957 PMCPMC2907411.
958 71. Haserick JR, Klein JA, Costello CE, Samuelson J. Cryptosporidium parvum vaccine candidates are
959 incompletely modified with O-linked-N-acetylgalactosamine or contain N-terminal N-myristate and S-
960 palmitate. PLoS One. 2017;12(8):e0182395. Epub 2017/08/10. doi: 10.1371/journal.pone.0182395. PubMed
961 PMID: 28792526; PubMed Central PMCID: PMCPMC5549699.
962 72. Van Dellen KL, Chatterjee A, Ratner DM, Magnelli PE, Cipollo JF, Steffen M, et al. Unique
963 posttranslational modifications of chitin-binding lectins of Entamoeba invadens cyst walls. Eukaryot Cell.

964 2006;5(5):836-48. Epub 2006/05/10. doi: 10.1128/EC.5.5.836-848.2006. PubMed PMID: 16682461; PubMed
965 Central PMCID: PMCPMC1459681.
966 73. Kang AY, Park AY, Shin HJ, Khan NA, Maciver SK, Jung SY. Production of a monoclonal antibody against
967 a mannose-binding protein of Acanthamoeba culbertsoni and its localization. Exp Parasitol. 2018;192:19-24.
968 Epub 2018/07/22. doi: 10.1016/j.exppara.2018.07.009. PubMed PMID: 30031120.
969 74. Kim DY, Son DH, Matin A, Jung SY. Production of a monoclonal antibody against a galactose-binding
970 protein of Acanthamoeba castellanii and its cytotoxicity. Parasitol Res. 2021;120(11):3845-50. Epub
971 2021/09/26. doi: 10.1007/s00436-021-07321-6. PubMed PMID: 34561750.
972 75. Kim MJ, Chu KB, Lee HA, Quan FS, Kong HH, Moon EK. Detection of Acanthamoeba spp. using
973 carboxylesterase antibody and its usage for diagnosing Acanthamoeba-keratitis. PLoS One.
974 2022;17(1):e0262223. Epub 2022/01/06. doi: 10.1371/journal.pone.0262223. PubMed PMID: 34986189;
975 PubMed Central PMCID: PMCPMC8730387.
976 76. Weber-Lima MM, Prado-Costa B, Becker-Finco A, Costa AO, Billilad P, Furst C, et al. Acanthamoeba spp.
977 monoclonal antibody against a CPA2 transporter: a promising molecular tool for acanthamoebiasis diagnosis
978 and encystment study. Parasitology. 2020;147(14):1678-88. Epub 2020/09/22. doi:
979 10.1017/S0031182020001778. PubMed PMID: 32951614; PubMed Central PMCID: PMCPMC10317748.
980 77. Aykur M, Karakavuk M, Akil M, Can H, Doskaya M, Guruz AY, et al. Development and Sensitivity
981 Determination of 18S rRNA Gene-specific Fast Loop-mediated Isothermal Amplification (LAMP) Assay for Rapid
982 Detection of Acanthamoeba. Turkiye Parazitol Derg. 2023;47(3):129-35. Epub 2023/09/19. doi:
983 10.4274/tpd.galenos.2023.46362. PubMed PMID: 37724360.
984 78. Mewara A, Khurana S, Yoonus S, Megha K, Tanwar P, Gupta A, et al. Evaluation of loop-mediated
985 isothermal amplification assay for rapid diagnosis of Acanthamoeba keratitis. Indian J Med Microbiol.
986 2017;35(1):90-4. Epub 2017/03/18. doi: 10.4103/ijmm.IJMM_16_227. PubMed PMID: 28303825.
987 79. Samuelson J, Robbins PW. Effects of N-glycan precursor length diversity on quality control of protein
988 folding and on protein glycosylation. Semin Cell Dev Biol. 2015;41:121-8. Epub 2014/12/06. doi:
989 10.1016/j.semcdb.2014.11.008. PubMed PMID: 25475176; PubMed Central PMCID: PMCPMC4452448.
990 80. Aurrecoechea C, Barreto A, Brestelli J, Brunk BP, Caler EV, Fischer S, et al. AmoebaDB and
991 MicrosporidiaDB: functional genomic resources for Amoebozoa and Microsporidia species. Nucleic Acids Res.
992 2011;39(Database issue):D612-9. Epub 2010/10/27. doi: 10.1093/nar/gkq1006. PubMed PMID: 20974635;
993 PubMed Central PMCID: PMCPMC3013638.
994 81. Marchler-Bauer A, Derbyshire MK, Gonzales NR, Lu S, Chitsaz F, Geer LY, et al. CDD: NCBI's conserved
995 domain database. Nucleic Acids Res. 2015;43(Database issue):D222-6. Epub 2014/11/22. doi:
996 10.1093/nar/gku1221. PubMed PMID: 25414356; PubMed Central PMCID: PMCPMC4383992.
997 82. Krogh A, Larsson B, von Heijne G, Sonnhammer EL. Predicting transmembrane protein topology with a
998 hidden Markov model: application to complete genomes. J Mol Biol. 2001;305(3):567-80. Epub 2001/01/12.
999 doi: 10.1006/jmbi.2000.4315. PubMed PMID: 11152613.
000 83. Eisenhaber B, Bork P, Eisenhaber F. Prediction of potential GPI-modification sites in proprotein
001 sequences. J Mol Biol. 1999;292(3):741-58. Epub 1999/09/25. doi: 10.1006/jmbi.1999.3069. PubMed PMID:
002 10497036.
003 84. Rigsby RE, Parker AB. Using the PyMOL application to reinforce visual understanding of protein
004 structure. Biochem Mol Biol Educ. 2016;44(5):433-7. Epub 2016/06/01. doi: 10.1002/bmb.20966. PubMed
005 PMID: 27241834.
006

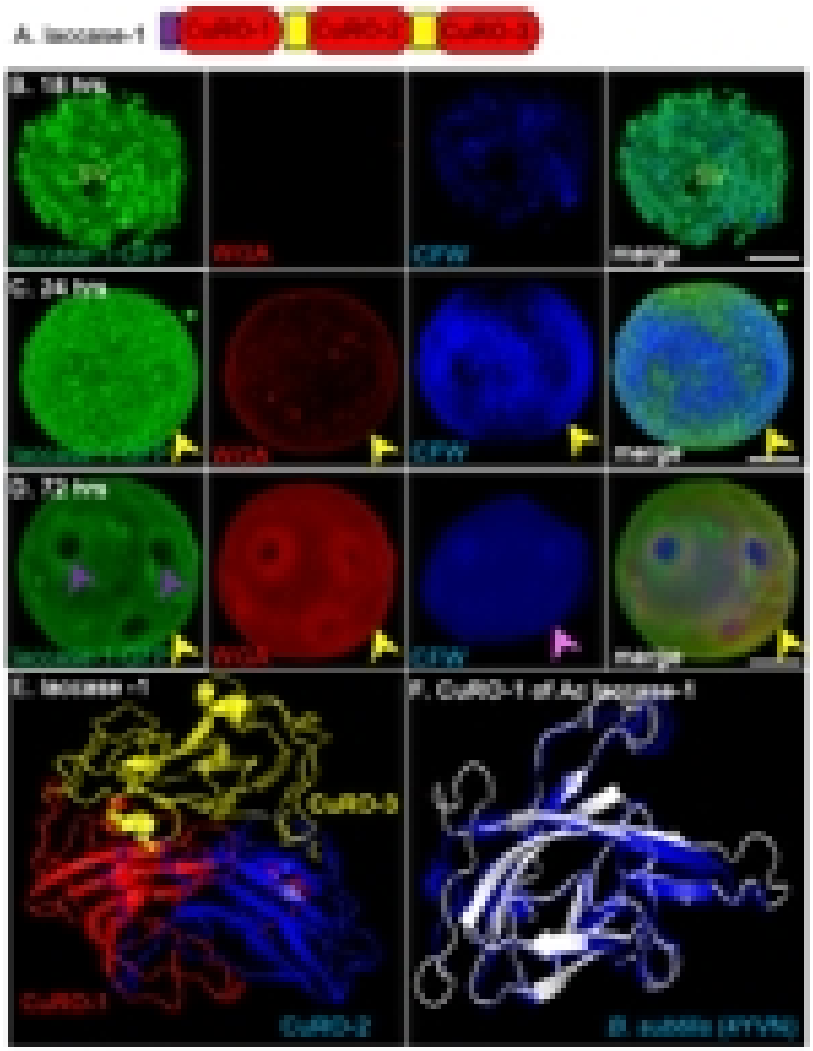
A. laccase-1
CuRD-1
CuRD-2
CuRD-3
B. 18 hrs
C. 24 hrs
D. 72 hrs
CFW
merge
E. laccase -1
CuRD-3
CuRD-1
CuRD-2
F. CuRD-1 of Ac laccase-1

Fig 4.

Fig 4

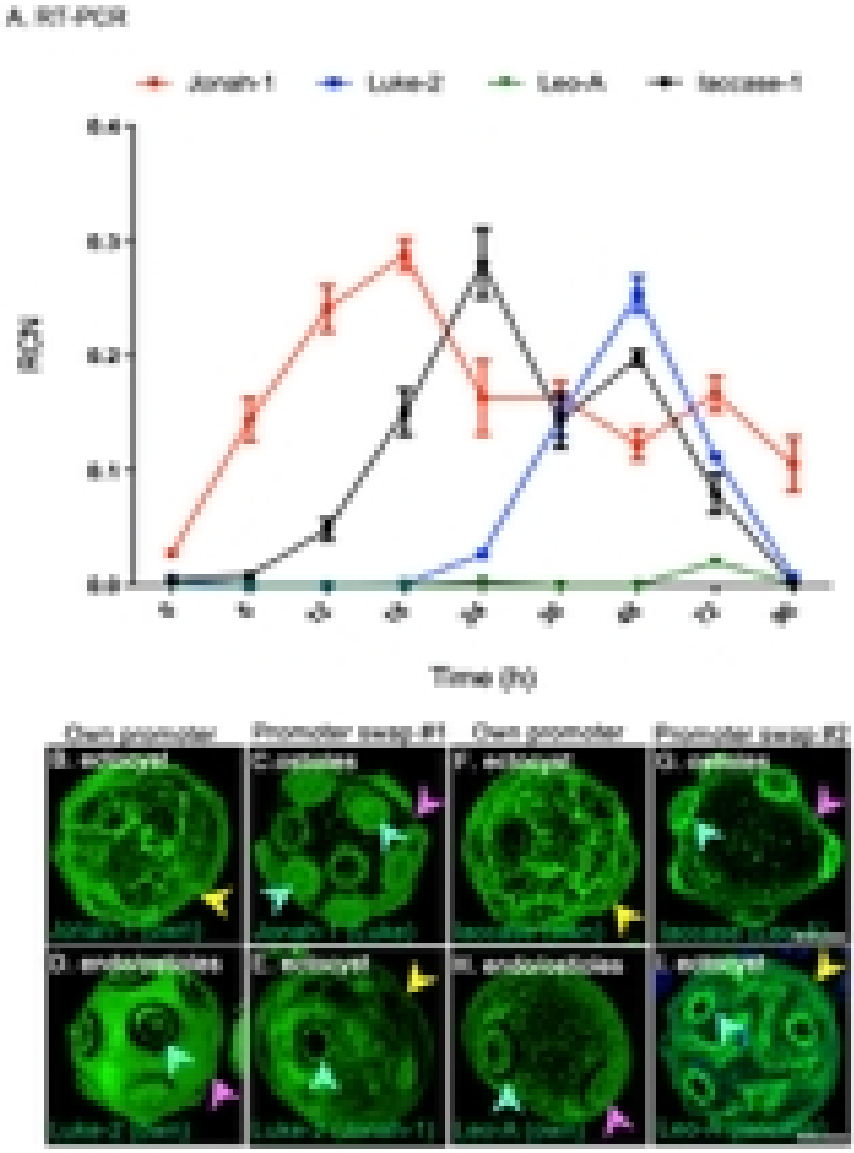
A. RT-PCR
Jonah-1
Luke-2
Leo-A
Iaccase-1
RCN
Time (h)
Own promoter
Promoter swap-#1
Own promoter
Promoter swap-#2

Fig 5.

Fig 5

A. Western blots of rAbs binding to trophozoites and cysts

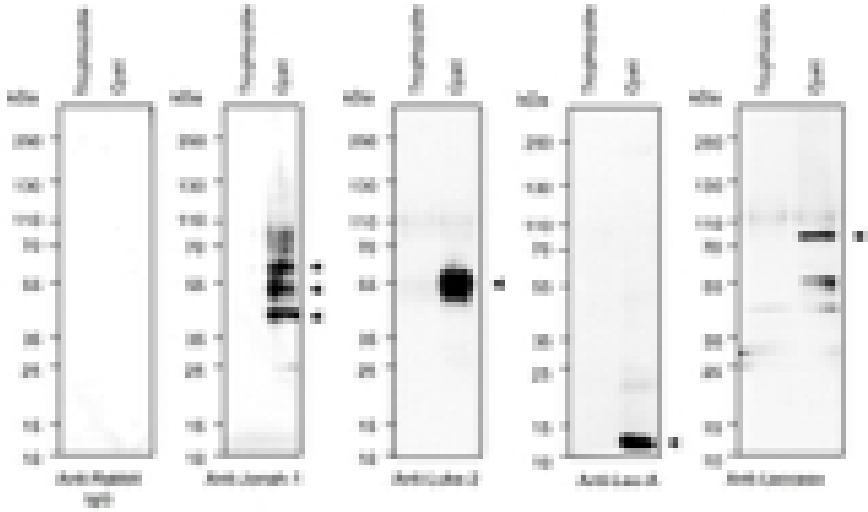

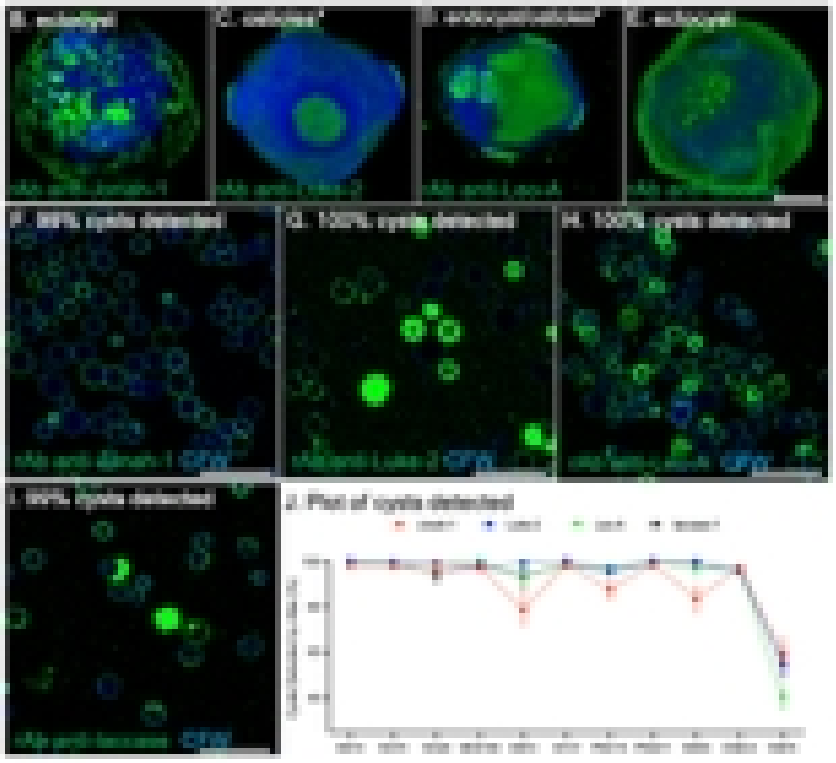

Fig 6.

Fig 6

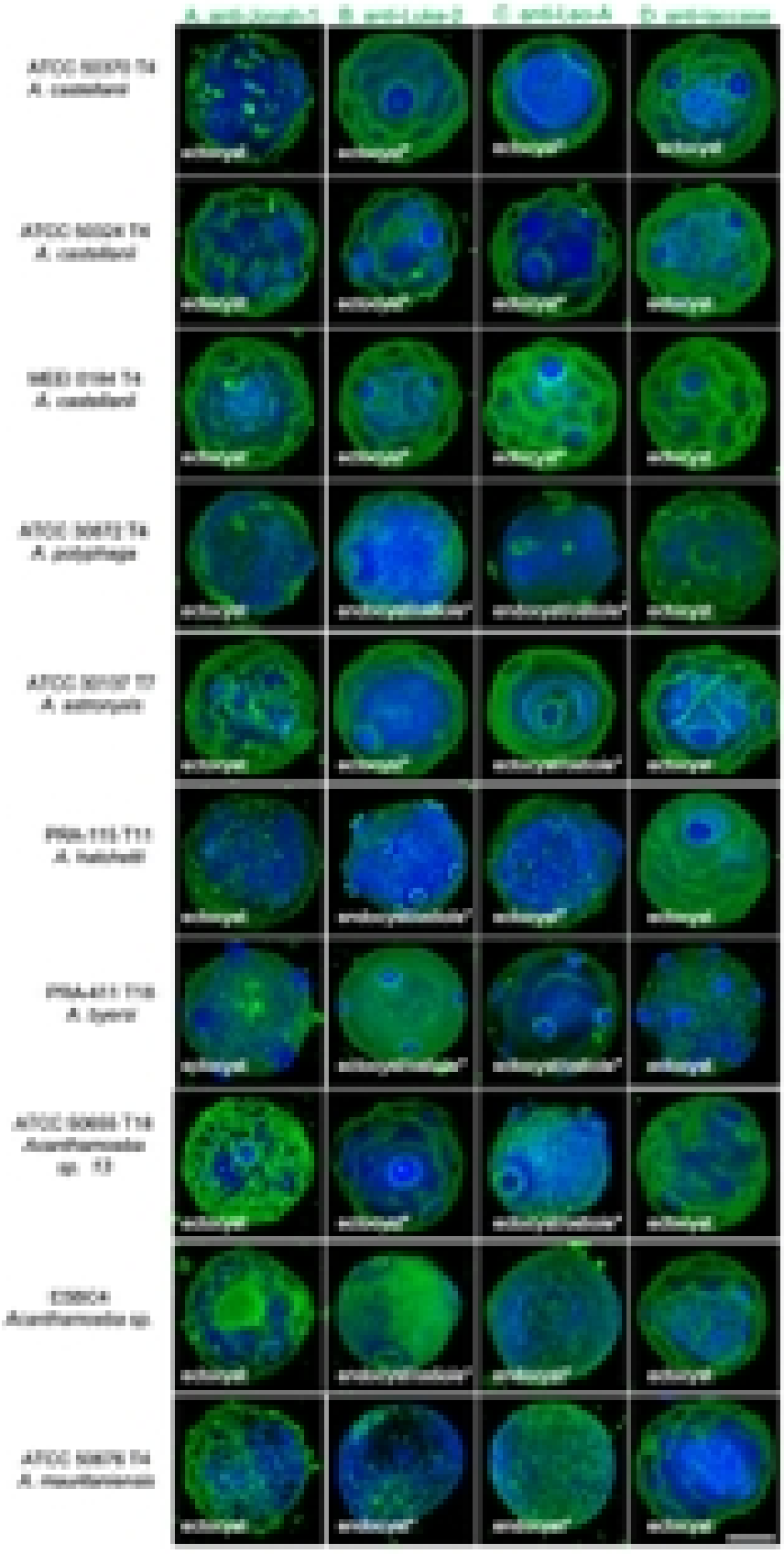

Fig 7.

Fig 7

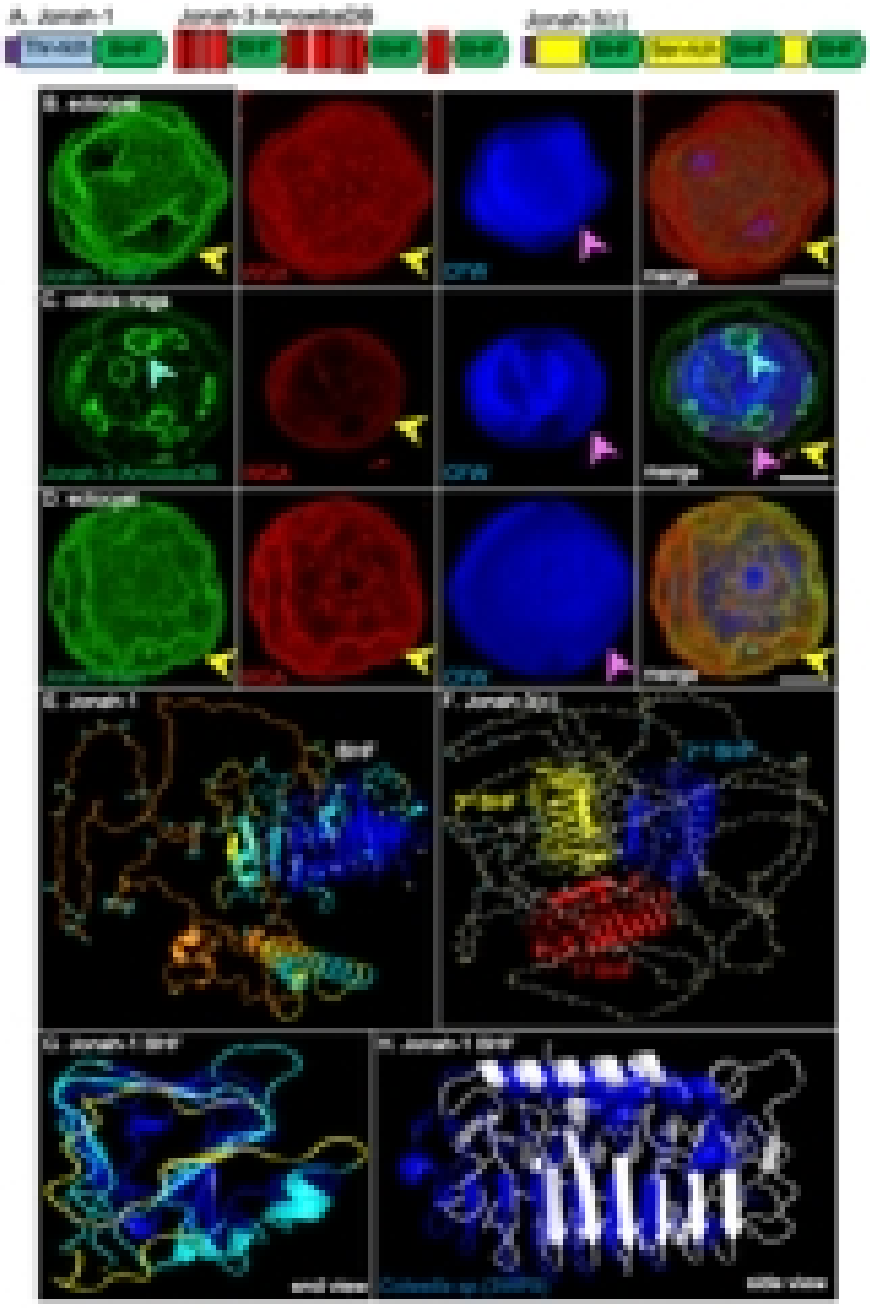

Fig 1.

Fig 1

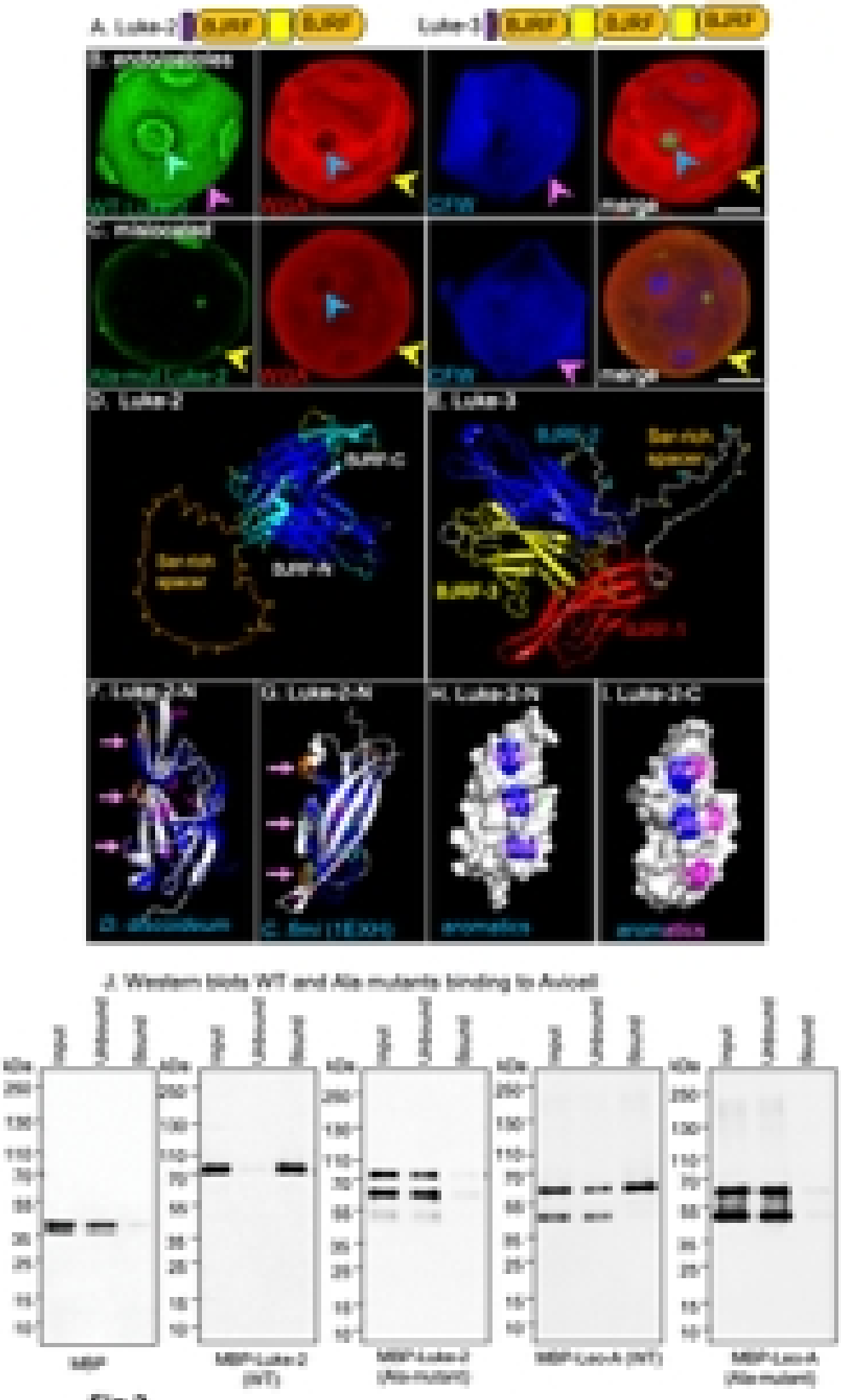
A. Luke-2
SURF
SURF
Luke-3
SURF
SURF
SURF
B. endolysosomes
WGA
CFW
merge
C. mislocated
Ala-mut Luke-2
WGA
CFW
merge
D. Luke-2
SURF-C
Ser-rich spacer
SURF-A
E. Luke-3
SURF-2
Ser-rich spacer
SURF-1
F. Luke-2-N
G. Luke-2-N
H. Luke-2-N
I. Luke-2-C
aromatics
aromatics
J. Western blots WT and Ala mutants binding to Avicell
Input
Unbound
Bound
kDa
250
130
110
70
55
35
25
15
10
MBP
MBP-Luke-2 (WT)
MBP-Luke-2 (Ala-mutant)
MBP-Leo-A (WT)
MBP-Leo-A (Ala-mutant)

Fig 2.

Fig 2

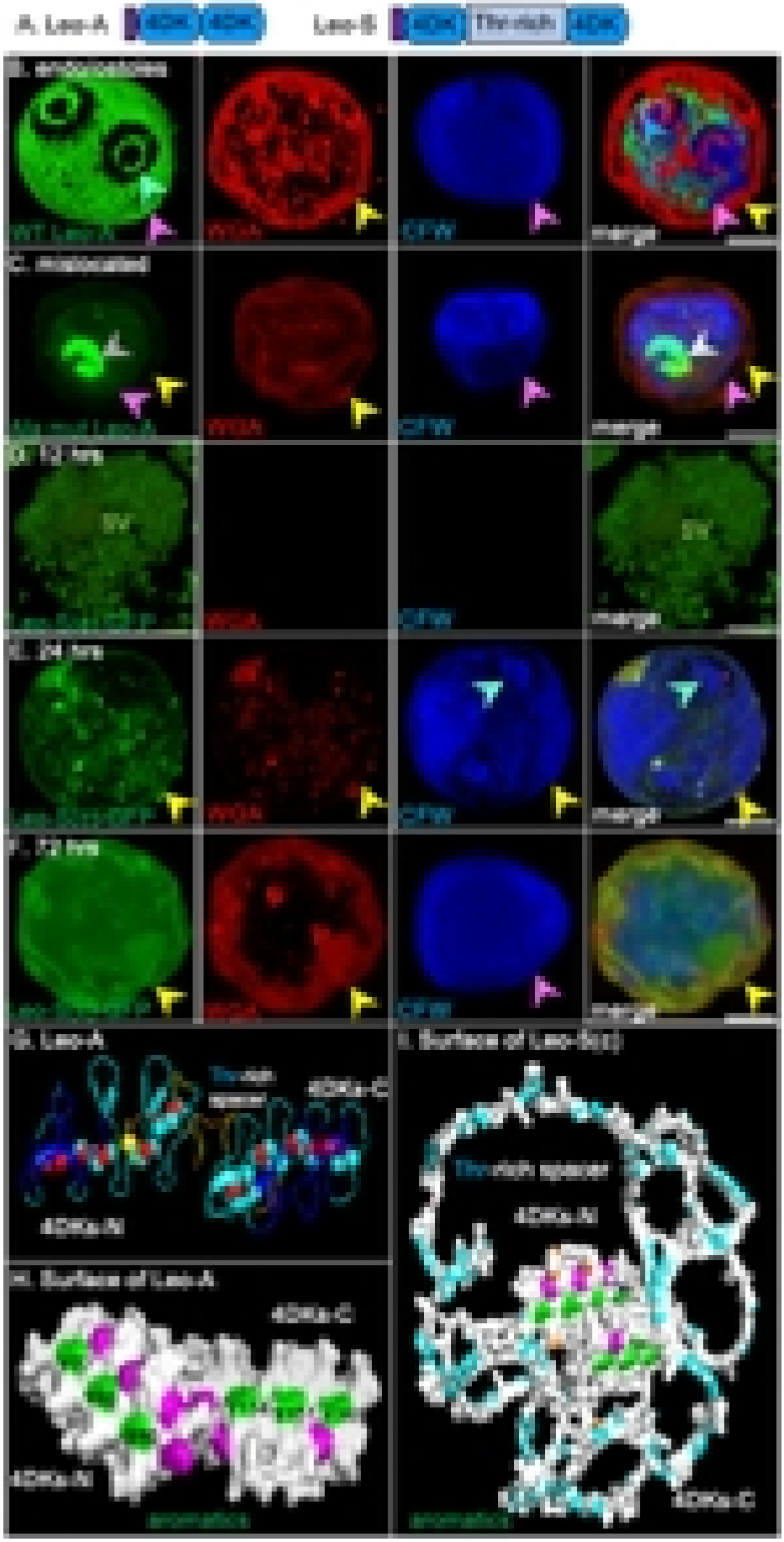
A. Leo-A
40K
40K
Leo-B
40K
Thr-rich
40K
B. endocytosis
WT Leo-A
WGA
CFW
merge
C. mislocated
Mis-mut Leo-A
WGA
CFW
merge
D. 12 hrs
SV
Leo-A-GFP
WGA
CFW
merge
E. 24 hrs
Leo-A-GFP
WGA
CFW
merge
F. 72 hrs
Leo-A-GFP
WGA
CFW
merge
G. Leo-A
Thr-rich spacer
40Ka-C
40Ka-N
H. Surface of Leo-A
40Ka-C
40Ka-N
electrostatics
I. Surface of Leo-b(c)
Thr-rich spacer
40Ka-N
40Ka-C
electrostatics

Fig 3.